Quarterly Journal of the Royal Meteorological Society
A journal of the atmospheric sciences and physical oceanography
RMetS Royal Meteorological Society

On the Role of Rossby Wave Breaking in the Quasi-Biennial Modulation of the Stratospheric Polar Vortex during Boreal Winter

Journal:	*QJRMS*
Manuscript ID	QJ-19-0147.R1
Wiley - Manuscript type:	Research Article
Date Submitted by the Author:	31-Oct-2019
Complete List of Authors:	Lu, Hua; British Antactic Survey, Hitchman, Matt; University of Wisconsin, Madison, Atmosphere and Ocean Sciences Gray, Lesley; University of Oxford, AOPP Anstey, James; Atmospheric, Oceanic and Planetary Physics, Department of Physics, University of Oxford, Osprey, Scott; Univ Oxford, Department of Physics
Keywords:	Dynamic/Processes < 1. Tools and methods, Dynamics < 3. Physical phenomenon, Stratosphere < 4. Geophysical sphere, Quasi-biennial oscillation, stratospheric polar vortex, Rossby wave breaking, Holton-Tan effect
Country Keywords:	United Kingdom Of Great Britain And Northern Ireland

Graphical Table of Contents

Title: ***On the Role of Rossby Wave Breaking in the Quasi-Biennial Modulation of the Stratospheric Polar Vortex during Boreal Winter***

Authors: ***Hua Lu*, Matthew H. Hitchman, Lesley J. Gray, James A. Anstey and Scott M. Osprey***

Key findings:

- Rossby wave breaking (RWB) is enhanced when the zero-wind line is shifted into the winter hemisphere by the Quasi-Biennial Oscillation (QBO) and where the QBO-induced meridional circulation is directed northward

- Polar vortex response to RWB differ in the lower and upper stratosphere in terms of seasonal development, latitudinal/heights location and zonal wavenumbers of the disturbances

- A cumulative effect of RWB in the upper to middle stratosphere manifests in a sign reversal of the Holton-Tan effect (HTE) in late winter

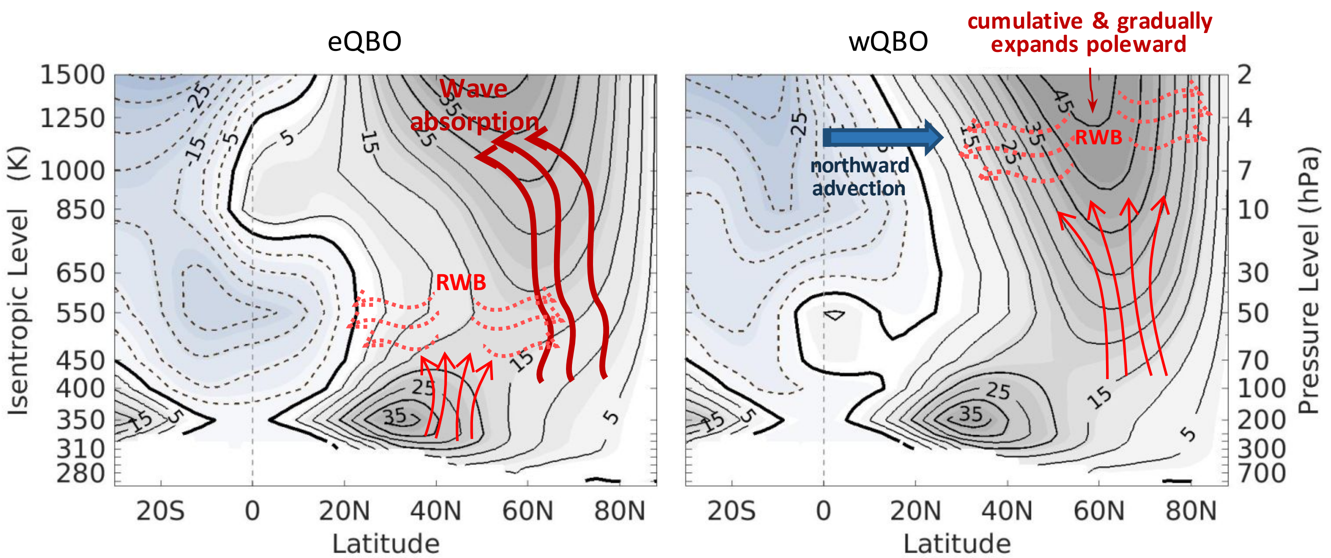

Schematic diagram showing the key features of RWB during eQBO (a) and wQBO (b) winters. Regions of RWB are indicated red-solid upward pointing arrows with meridional dotted-wiggled arrows above. The thick-solid upward wiggling arrows that extend from the lower stratosphere into upper stratosphere indicate enhanced upward wave propagation and absorption. The northward pointing blue arrow indicate enhanced cross-equatorial flow.

On the Role of Rossby Wave Breaking in the Quasi-Biennial Modulation of the Stratospheric Polar Vortex during Boreal Winter

Hua Lu[1,a], Matthew H. Hitchman[b], Lesley J. Gray[c], James A. Anstey[d] and Scott M. Osprey[c]

Revised for ***Quarterly Journal of the Royal Meteorological Society***

21-10-2019

---

[1]Corresponding author Email: hlu@bas.ac.uk

[a] *British Antarctic Survey, High Cross, Madingley Road, Cambridge CB3 0ET, United Kingdom. (hlu@bas.ac.uk)*

[b] *Department of Atmospheric and Oceanic Sciences, University of Wisconsin – Madison, 1225 West Dayton Street Madison, WI 53706, USA (matt@aos.wisc.edu)*

[c] *NCAS-Climate, Department of Atmospheric Physics, Oxford University, Clarendon Laboratory, Parks Road, Oxford, OX1 3PU, United Kingdom (gray@atm.ox.ac.uk; Scott.Osprey@physics.ox.ac.uk)*

[d] *Canadian Centre for Climate Modelling and Analysis, Environment and Climate Change Canada, Victoria, British Columbia, Canada (james.anstey@canada.ca)*

Abstract: The boreal-winter stratospheric polar vortex is more disturbed when the quasi-biennial oscillation (QBO) in the lower stratosphere is in its easterly phase (eQBO), and more stable during the westerly phase (wQBO). This so-called "Holton-Tan effect" (HTE) is known to involve Rossby waves (RWs) but the details remain obscure.

This tropical-extratropical connection is re-examined in attempt to explain its intra-seasonal variation and its relation to Rossby wave breaking (RWB). Reanalyses in isentropic coordinates from the National Center for Environmental Prediction Climate Forecast System covering the entire stratosphere and for the 1979 – 2017 period are used to evaluate the relative importance of RWB in the context of extratropical waveguide, wave absorption, and the QBO-induced meridional circulation. During eQBO, the net wave forcing on the polar vortex is enhanced in early winter mainly due to ~25% increase in upward propagating zonal wavenumber 1. RWB is also enhanced in the lower stratosphere. The effect is characterized by convergent anomalies in the subtropics and at high-latitudes in response to more positive meridional gradients of potential vorticity (PV) in the subtropical to mid-latitudes. During wQBO winters, RWB in association with zonal wavenumbers 2 and 3 is enhanced in the middle to upper stratosphere. During November to January, RWB acts to sharpen PV gradients near the polar vortex edge, resulting in a stable polar vortex. As the winter progresses, RWB gradually "erodes" the polar vortex. A poleward confinement of wave activity results in a more disturbed polar vortex in February – March, thus the observed weakening and/or a sign reversal of the HTE in late winter.

Keywords: Quasi-biennial oscillation; stratospheric polar vortex; Rossby wave breaking; Holton-Tan effect.

1. Introduction

The polar vortex is the westerly circumpolar jet in the winter stratosphere, which owes its existence to the equator-to-pole temperature gradient (Andrews *et al*., 1987). The vortex varies in strength in response to upward propagation of planetary-scale Rossby waves (PRWs) emanating from the troposphere (Scherhag, 1952; Matsuno, 1970; 1971). Disturbances due to PRWs can result in extreme vortex events, i.e. stratospheric sudden warmings (SSWs), which are known to affect surface climate up to a few months (Baldwin and Dunkerton, 1999; Kidston *et al*., 2015). It is important to capture stratosphere variability and the associated downward influences because it has been shown that incorporating stratospheric processes into forecast models can lead to improved weather prediction, especially on sub-seasonal to seasonal time-scales (e.g. Marshall and Scaife, 2009). The mechanism(s) are however not fully understood because the propagation of PRWs and their subsequent breaking and absorption by the background mean flow are influenced by other factors (McIntyre, 1982; Kidston *et al*., 2015).

The factors that are known to influence PRWs include the El Niño/Southern Oscillation (e.g. Domeisen *et al*., 2019), major volcanic eruptions (e.g. Kodera, 1994; Robock, 2000), Eurasian snow cover extent or Artic sea-ice (Cohen and Entekhabi, 1999; Nakamura *et al*., 2016; Labe *et al*., 2019), solar ultraviolet irradiance (e.g. Gray *et al*., 2010; Lu *et al*., 2017) and the quasi-biennial oscillation (QBO) (Baldwin *et al*., 2001; Gray *et al*., 2018). The QBO is a tropical phenomenon characterized by alternating descending easterly and westerly winds with a period ranging from 24 to 32 months (Baldwin *et al*., 2001; Schenzinger *et al*., 2017). Holton and Tan (1980) found that the boreal-winter stratospheric polar vortex was more disturbed when the QBO in the lower stratosphere was in its easterly phase but remains stable when the QBO was in its westerly phase. This so-called "Holton-Tan effect" (HTE) has been linked to the occurrence and/or timing of SSWs, with SSWs occurring more frequently during the easterly QBO winters than westerly QBO winters (Labitzke, 1982; Dunkerton and Baldwin, 1991; Gray *et al*., 2004). The strength of the HTE also varies on multi-decadal time-scales and is further affected by the 11-year solar cycle (Gray *et al.*, 2004; Lu *et al.*, 2008; 2014).

The classic mechanism hypothesized for the HTE involves changes in the winter stratospheric waveguide in response to a latitudinal shift of the zero-wind line near the equator by the QBO (Holton and Tan, 1980). When the QBO is in its easterly phase, the zero-wind line is shifted into the subtropical winter hemisphere. PRWs are thus confined more towards the extratropical winter stratosphere and the vortex weakens in response to this enhanced wave forcing. Conversely, when the QBO is in its westerly phase, the zero-wind line is in the summer hemisphere. A wider than normal waveguide in the winter hemisphere results in a less disturbed polar vortex.

Studies aimed at verifying this classic mechanism have so far been inconclusive (see Anstey and Shepherd, 2014 for a review). For instance, when the QBO is in its easterly phase, the refractive index for stationary PRWs increases in the subtropics and at high latitudes but reduces in the mid-latitudes where the polar-vortex westerlies maximize (Lu *et al.*, 2014). QBO modulation of wave mean-flow interaction differs from the lower and upper stratospheres (Yamashita *et al.*, 2011; Garfinkel *et al.*, 2012). These QBO-related changes cannot be fully explained by the classic mechanism. Furthermore, the December–February averaged upward Eliassen-Palm (EP) fluxes F_z in the mid-latitude lower stratosphere was found to differ comparatively little between the two QBO phases (e.g. Baldwin and Dunkerton, 1991; Calvo *et al.*, 2007). Instead, the QBO anomaly in F_z in the lower stratosphere appeared to reverse in sign between early and late winter (e.g. Hitchman and Huesmann, 2009 (HH09); Naoe and Shibata, 2010; White *et al.*, 2016). F_z of zonal wavenumber 1 was enhanced in early winter when the QBO was in its easterly phase, but an enhancement of zonal wavenumber 2 was detected in late winter in assocaition with the westerly QBO (Hu and Tung, 2002; Ruzmaikin *et al.*, 2005).

It has been suggested that changes in the zero-wind line location may also alter extratropical wave forcing via poleward wave reflection (Tung, 1979; Holton and Tan, 1982). Watson and Gray

(2014) studied this effect using a climate model and found anomalous poleward wave propagation from the height region where the QBO zero-wind line is located in the winter hemisphere. However, such a response could only be observed during the first few days of the model integration. Zonal winds in the equatorial upper stratosphere in determining polar vortex variability have also been reported (Gray *et al*., 2003; Pascoe *et al*., 2006). When easterly wind anomalies were imposed in the equatorial upper stratosphere, the disruption to the polar vortex tends to occur earlier than average (Gray *et al*., 2003). Pascoe *et al.* (2006) later found that the main impact of the equatorial upper stratospheric wind anomaly was on the timing of SSWs; SSWs were delayed when the zonal winds in the equatorial upper stratosphere were strong westerlies while SSWs occurs earlier when easterly anomalies are found in the equatorial or subtropical upper stratosphere. The importance of QBO-induced changes in EP-flux convergence in the middle to upper stratospherehave also been reported by other studies (e.g. Calvo *et al.,* 2007; Garfinkel *et al*., 2012; Lu *et al*., 2014).

Studies have also suggested that the QBO-induced mean meridional circulation (QBO-MMC) plays an important role in the HTE (Ruzmaikin *et al*., 2005; Gray *et al*., 2004; Garfinkel *et al*., 2012). Garfinkel *et al*. (2012) performed model simulations by imposing the QBO at the equator. They found that synoptic-scale Rossby waves (SRWs) are enhanced in the subtropical lower stratosphere during easterly-QBO winters. Breaking of SRWs in the vicinity of the subtropical westerly jet (SWJ) results in a poleward expansion of the region with positive meridional gradients of potential vorticity (PV) (Garfinkel and Hartmann, 2011). More PRWs are able to enter the extratropical stratosphere as a result. The increase of SRWs in the subtropical lower stratosphere during easterly QBO winters was attributed to the QBO-MMC (Garfinkel and Hartmann, 2011; Garfinkel *et al*., 2012). However, using a reanalysis data set, White et al. (2016) found that the increase in SRWs in the subtropical lower stratosphere was only statistically significant in late winter when the HTE is weak. Furthermore, Gray *et al.* (2003) and Naito and Yoden (2006) imposed easterly wind anomalies to encompass the entire tropics between the lower stratosphere and the lower mesosphere, effectively remove the QBO-MMC. A "HTE-like" response was also detected.

Upward propagating PRWs through the stratosphere are normally refracted equatorward; there they encounter the zero-wind line that separates the westerly winds in the winter hemisphere from the tropical easterlies. Changes in wave absorption or reflection near the zero-wind line would alter the net wave forcing on the polar vortex (Tung, 1979; Killworth and McIntyre, 1985). In the context of the HTE, we would expect QBO-altered zero-wind line to affect meridional wave transport via Rossby wave breaking (RWB), which is a common phenomenon in the winter stratosphere. During a RWB event, filaments of air are stripped from the polar vortex edge and mixed into the surrounding region (McIntyre and Palmer, 1983; 1984; Leovy *et al*., 1985). Wave disturbances can also span from the tropical zero-wind line to the polar vortex, providing a direct means of coupling between low and high latitudes (O'Sullivan and Salby, 1990).

An individual RWB event is rarely responsible for an immediate break down of the polar vortex, either minor or major SSWs (McIntyre, 1982; Greer *et al*., 2013). Recurrent RWB events reshape the geometry of the stratospheric waveguide and lead to the formation of the surf zone. When the upward propagating waves are of relatively small amplitude, RWB acts to sharpen PV gradients along the vortex edge while irreversible mixing takes place on the equatorward flank of the polar vortex. In the early stage of the development, the region with sharpened PV gradients makes the vortex resistant to further wave disturbances, thus maintaining a stable vortex (Polvani and Saravanan, 2000; Scott and Dritschel, 2005). A sudden, rapid intrusion of low-PV-air into the polar region can take place if the surf zone expands continuously poleward as RWB builds up cumulatively (Polvani and Saravanan, 2000; Albers and Birner, 2014). RWB initialized at upper levels may also gradually extend downward into lower levels to destroy the polar vortex completely (Waugh and Dritschel, 1999; Polvani and Saravanan, 2000). As such, RWB is thought to 'precondition' the polar vortex, making it more susceptible to SSWs at a later stage (Limpasuvan *et* *al*., 2004; Albers and Birner, 2014). These characteristics make RWB differing from the linear theory that accounts for direct wave absorption at the polar vortex edge (Matsuno, 1971).

A large number of studies have been carried out to characterize RWB and its climatology at different height regions (e.g. Hitchman and Huesmann, 2007; Abatzoglou and Magnusdottir, 2007; Greer *et al*., 2013). For instance, it is found that stratospheric RWB can be broadly classified into upper-level events where PRWs propagate along the polar vortex edge and break in the upper stratosphere and lower-level events where RWB is confined to the lower stratosphere (Abatzoglou and Magnusdottir, 2007). The upper-level RWB occurs more often in early winter while the lower-level RWB dominates in middle winter. Only a limited number of studies have been devoted to examine the role of RWB in the HTE and its seasonal variation. HH09 calculated the statistics of RWB based on ERA-40 reanalysis data from ECMWF (European Centre for Medium-range Weather Forecasts) over the 1979–2002 period. They found that during December to February, meridional PV gradients in the subtropical lower stratosphere were enhanced during easterly QBO winters while the frequency RWB was reduced in the same region but enhanced above that level. These results were later confirmed by White *et al.* (2015; 2016) using the Interim dataset from ECMWF on isentropic coordinates. It was shown that the QBO-related waveguide and wave activity anomalies extended from the subtropics into high latitudes, implying an important role of RWB. However, the analyses of White *et al.* (2015; 2016) were confined to the height region between 350 K and 850 K (~100-10 hPa). RWB in the upper stratosphere and its role in the HTE were left unexamined.

The aim of this paper is to provide a more complete picture of the HTE with an improved description of RWB that encompasses the entire stratosphere. A set of diagnostics are performed to examine QBO-related changes in RWB with a special attention paid to its cumulative effect on the polar vortex. The relative importance of RWB is evaluated in the context of extratropical waveguide, wave forcing on the polar vortex, and the QBO-MMC. Contributions from PRWs and

SRWs are separately assessed, which allows us to better compare the effect of RWB to wave absorption near the polar vortex edge. A new mechanism is then proposed to explain the observed intra-seasonal variation of the HTE, especially its late winter weakening and/or sign reversal.

2. *Data and Methods*

2.1. Diagnostics

Ertel's PV in isentropic coordinates provides useful information on the structure and evolution of winter stratospheric dynamics (Hoskins *et al.*, 1985). It is given by

$$P = \xi / \sigma \qquad (1)$$

where σ is the isentropic density, $\xi = f - \frac{(u\cos\phi)_\phi}{a\cos\phi} + \frac{v_\lambda}{a\cos\phi}$ is the vertical component of absolute isentropic vorticity, f the Coriolis parameter. a the Earth's radius, u, v the zonal and meridional velocities, ϕ latitude, and λ the longitude. PRWs preferentially propagate towards the region where the zonally averaged meridional PV gradient $\overline{P}_\phi$ is large. $\overline{P}_\phi$ is thus used here as a diagnostic for the stratospheric waveguide.

RWB is diagnosed by overturning contours of PV on isentropic surfaces, which is related to momentum deposition of PRWs via RWB (McIntyre and Palmer, 1983; 1984; HH09). Following HH09, RWB frequency is estimated by counting the number of days in which the meridional gradient of Ertel's PV ($\overline{P}_\phi$) becomes negative at each grid point during a pre-selected month or season. The zonal-mean is then taken of this grid-point metric. This zonal-mean metric is denoted as $\overline{\gamma}$ hereinafter and has the units of days per month or season. $\overline{\gamma}$ allows us to examine the extent to which the QBO modulates RWB in terms of relative frequency, location and timing in a statistically averaged sense. $\overline{\gamma}$ does not provide a detailed accounting of the individual events including the size, strength, or duration. This is justified for our purpose as our aim is to compare the relative importance of RWB events between the two QBO phases.

Analyses of $\overline{P}_{\phi}$ and $\overline{\gamma}$ are supplemented by additional diagnostics including the Eliassen-Palm (EP) fluxes and divergence, and down-gradient eddy PV fluxes. Following Andrews *et al.* (1987), the meridional and vertical components of the EP flux in isentropic coordinates are estimated by

$$\begin{aligned}\tilde{F}^{(\phi)} &= -a\cos\phi\,\overline{(\sigma v)'u'} \\ \tilde{F}^{(\theta)} &= g^{-1}\,\overline{p'\Psi'_{\lambda}} - a\cos\phi\,\overline{(\sigma Q)'u'}\end{aligned} \tag{2}$$

where θ is potential temperature, g the gravitational acceleration constant, p pressure, Ψ the Montgomery stream-function, and Q the diabatic heating rate. Overbars denotes zonal averaging on an isentropic surface, subscripts denote derivatives with respect to the given variable, and primes denote departures from the zonal-mean.

The EP flux divergence $(a\cos\phi)^{-1}\tilde{\nabla}\cdot\tilde{\mathbf{F}} = (a\cos\phi)^{-2}\dfrac{\partial}{\partial\phi}\left(\tilde{F}^{(\phi)}\cos\phi\right) + (a\cos\phi)^{-1}\dfrac{\partial\tilde{F}^{(\theta)}}{\partial\theta}$ is commonly used to diagnose wave forcing on the mean flow. It is generally in balance with the residual-mean circulation as other terms in momentum budget equations tend to be one order of magnitude small in seasonal averages (Andrew *et al*., 1987). Studies have found that RWB-related disturbances in the upper stratosphere invole local acceleration/deccelaration and the circulation there is effectively non-geostrophic (e.g. Greer *et al*., 2013). An alternative form of wave forcing in isentropic coordinates that better accounts for ageostrophic motion can be expressed as the density-weighted eddy PV flux on isentropic surfaces (Tung 1986; Andrew *et al*., 1987):

$$\Pi = \overline{\sigma}\,\overline{\hat{v}\hat{P}}^{*} \tag{3}$$

where the overbar with an asterisk denotes the quantity is a density weighted zonal mean, i.e. $\overline{v}^{*} = \overline{\sigma v}/\overline{\sigma}$ and a caret denotes the departure from the density-weighted zonal average, i.e. $\hat{v} = v - \overline{v}^{*}$. Similar to the EP flux divergence, Π represents the wave forcing per unit of mass on the mean flow and has the units of m s^{-1} day^{-1}. Negative values of Π indicate wave convergence. Thus, disturbances of PRWs act to slow down the background westerlies and the northward residual mean circulation is expected to be strong due to enhanced wave forcing on the mean flow. In this study, $\tilde{F}^{(\phi)}$, $\tilde{F}^{(\theta)}$ and Π are used together to assess PRW propgation and wave driving. These quantities are further separated into contributions from planetary waves of zonal wavenumber 1, 2-3 and synoptic-scale Rossby waves (SRWs) where zonal wavenumbers 5-10 are included.

Meridional transfer of wave activity between the polar vortex edge and the subtropics during RWB events induces changes in enstrophy, i.e. $\overline{P'^2}/2$ (McIntyre and Palmer, 1983). Away from the zero-wind line where the linear wave thoery may break down, the meridional exchange of enstrophy is largely determined by down-gradient eddy PV fluxes (Schoeberl and Smith, 1986; White *et al*., 2015):

$$\Gamma = \bar{P}_\phi \overline{\hat{v}\hat{P}}^* / a \tag{4}$$

which is effectively the product of the wave forcing Π and meridional PV gradient $\bar{P}_\phi$. Given that $\bar{P}_\phi$ is generally positive and $\overline{\hat{v}\hat{P}}^*$ is largely negative in the winter stratosphere, Γ must be predominantly negative. Climatologically, we expect down-gradient transfer of PV fluxes to be most strong near the polar vortex edge because RWB acts to "strip off" high-PV airs from the polar vortex edge and "flux out" them sideways (McIntyre and Palmer, 1983; Schoeberl and Smith, 1986). Thus, large negative values of Γ should peak along the flanks of the polar vortex. Γ is used here to examine QBO-related changes in meridional wave transfer. For instance, in a region where Γ becomes more negative, it indicates wave growth due to enhanced influxes of enstrophy (see section 2c of White *et al*., 2015).

2.2. Global data sets and statistical analysis

The reanalysis data sets used are from the National Centers for Environmental Prediction (NCEP) and include the Climate Forecast System Reanalysis (CFSR) for the period of 1979-2010 and its extension - the Climate Forecast System version 2 (CFSv2) - covering the period 2011-2017

(Saha *et al*., 2012). Jointly, they cover the 1979-2017 period (39 years in total). Both data sets were generated by NCEP's Climate Forecast System (CFS), which assimilates standard ground-based, radiosonde, and satellite observations into an atmosphere-ocean general circulation model with fully coupled atmosphere, land, ocean and sea ice components. Observed carbon dioxide, aerosols, other trace gases and solar variations are also included. Currently, CFSR and CFSv2 are the only reanalysis products directly providing isentropic level data at altitudes above 850 K (~10 hPa or 32 km).

The 6-hourly isentropic level data output at 2.5° horizontal resolution on sixteen potential temperature levels from 270 K to 1500 K (equivalent to 900-2 hPa or 1-45 km) were obtained from http://rda.ucar.edu/datasets. Unlike previous studies that generated data on isentropic surfaces by interpolating 6-hrly pressure-level data provided by ECMWF (e.g. HH09; White *et al*., 2015; 2016), the isentropic level data used here were generated by NCEP as an integral part of the CFSR/CFSv2 reanalyses. The data used here involve no additional interpolation. All the diagnostics described in Section 2.1 are first calculated using daily averages of the 6-hourly fields before taking monthly and seasonal averages. The derivatives are calculated using centred differences except for the top and bottom isentropic levels where one-sided differences are used.

Previous studies suggest that the QBO defined by the tropical zonal winds near 40-50 hPa appears to optimize the stratospheric vortex response during NH winter (e.g. Holton and Tan, 1980; Lu *et al*., 2008; HH09; Gray *et al*., 2018). The monthly-averaged tropical zonal winds at 40 hPa and 50 hPa are obtained from radiosonde observations issued by the Freie Universität Berlin (Naujokat, 1986; FUB, 2016). Here, the easterly phase is defined for each individual month when the winds at both 40 hPa and 50 hPa are negative while the westerly phase is defined for each individual month when the equatorial winds at both pressure heights are positive. Additionally, the two years following the two major volcanic eruptions are excluded (i.e., El Chichón, March 1982 and Mount Pinatubo, June 1991). This results in eleven easterly QBO NH winters (i.e. 1979/80, 1981/82, 1984/85, 1989/90, 1996/97, 1998/99, 2003/04, 2005/06, 2007/08, 2012/13, 2014/15) and eighteen westerly QBO NH winters (i.e. 1980/81, 1985/86, 1987/88, 1988/89, 1990/91, 1993/94, 1995/96, 1997/98, 1999/00, 2002/03, 2004/05, 2006/07, 2008/09, 2010/11, 2011/2012, 2013/14, 2015/16, 2016/17). Note that there are more winters classified as wQBO than eQBO. This is because descending wQBO tends to stall and linger longer in the lower stratosphere while eQBO descends more quickly there. The dates listed may vary slightly from early to late winter as the QBO changes phase. Hereinafter the easterly and westerly QBO phase groups are denoted by eQBO and wQBO, respectively.

Note also that five wQBO winters coincide with ENSO events (i.e. 1997/98, 2002/03, 2004/05, 2006/07 and 2015/16) while only one eQBO winter was affected by a major ENSO event (i.e. 2014/15). We have carried out sensitivity tests by excluding those ENSO-affected winters and the results remain qualitatively the same (not shown).

The QBO signals are estimated based on the composite-mean differences between eQBO and wQBO subgroups (i.e. eQBO – wQBO). The statistical significance of eQBO – wQBO composite-mean differences is assessed using a Monte Carlo trial based non-parametric test. The procedure involves replacement of eQBO and wQBO composite members by randomly sub-sampling the original time series with replacement before averaging. This procedure is repeated 10,000 times and a distribution of the composite-mean differences is constructed. The original composite-mean difference estimated from the actual eQBO and wQBO subgroups is then compared with this distribution. When the actual positive (negative) difference is located within the upper (lower) 5% of the distribution, the difference is regarded as statistically significant and referred to as *the QBO signal*. Very similar results are obtainable based on Student's *t*-test (not shown).

3. *Results*

3.1. Mean-state and RWB responses

The climatological zonal-mean zonal winds $\overline{u}$ under eQBO and wQBO during November to January (Nov-Jan) and February to March (Feb-Mar) are shown in Fig. 1a-d. As expected, $\overline{u}$ in the NH is characterised by two westerly jets, i.e. the stratospheric polar vortex and the subtropical jet in the troposphere. The winter westerlies and summer easterlies are separated by the zero-wind line near the equator, where distinct differences between eQBO and wQBO are visible.

[[Insert Fig. 1 here]]

The QBO signal (i.e. eQBO – wQBO) in NH $\overline{u}$ during Nov-Jan is marked by easterly differences at high latitudes (up to -10 m s^{-1}) and westerly differences in the subtropics (~5 m s^{-1}) (Fig. 1e). Larger differences (~ ±35 m s^{-1}) can be found at the equator though the maximum/minimum colour values in Fig. 1e, f have been capped to ±15 m s^{-1} in order to highlight the extratropical responses. In late winter the sign of the response reverses, with westerly differences in the upper stratosphere at mid-high latitudes (~13 m s^{-1}) (Fig. 1f). Fig. 1 also indicate that the SWJ in the NH is weakened and/or shifted poleward under eQBO in late winter. These results are in good agreement with previous studies (Lu *et al*., 2014; White *et al*., 2016).

The corresponding QBO response of the zonal-mean temperature $\overline{T}$ is shown in Fig. 2. The QBO signal in extratropical $\overline{T}$ is marked by warm differences in the polar lower to middle stratosphere during Nov-Jan, and cold differences in the middle to upper stratosphereduring Feb-Mar. At low latitudes, the QBO signal is marked by a vertical tripole structure in the tropics and a dipole pattern in the subtropics, which are associated with the QBO-MMC (Plumb and Bell, 1982). Similar to the QBO signals in $\overline{u}$ (Fig. 1e, f), these low-latitude QBO signals in $\overline{T}$ also persist throughout the winter.

[[Insert Fig. 2 here]]

Figs. 1e and 2a confirms that the HTE holds most robustly in early winter (e.g. Gray *et al*., 2004; 2018; Lu *et al*., 2008; 2014; White *et al*., 2016). The late winter response however differs in significance and magnitude in comparison with previous studies. For instance, a weaker HTE in the lowermost stratosphere rather than a full sign reversal was obtained if pre-1979 data were included (see Figures 1e, f of Lu *et al*., 2014). Lu *et al*. (2014) found that a late-winter weakening or reversal of the HTE during 1977-1998 was associated with a distinctly stronger and/or wider polar vortex around Nov-Jan.

Fig. 3 shows the eQBO and wQBO composites of the zonal-mean PV gradient $\overline{P}_\phi$ and the corresponding QBO composite differences during Nov-Jan and Feb-Mar. As expected, the climatological $\overline{P}_\phi$ is mostly positive during both eQBO and wQBO winters (Fig. 3a-d). Large values of $\overline{P}_\phi$ are found at low latitudes where RWs tend to be absorbed and near the westerly jets where RWs preferably propagate towards (Matsuno, 1970). In the extratropical NH, the most preferable route for the upward propagating PRWs is the polar vortex edge (i.e. grey dotted lines in Fig. 3e. f). In the subtropical to mid-latitude lower stratosphere, i.e. 25-60°N, 350-550 K, RWs preferably propagate towards the equator; an effect that is most pronounced for SRWs (Karoly and Hoskins, 1982). Relatively small values of $\overline{P}_\phi$ are found in the latitude band of 20-45°N in the middle stratosphere where the surf zone is formed as a result of RWB (McIntyre and Palmer, 1983; Hitchman and Huesmann, 2007).

[[Insert Fig. 3 here]]

The extratropical QBO signal in $\overline{P}_\phi$ is dominated by negative differences at 55-75°N, 450-1000 K during Nov-Jan and positive $\overline{P}_\phi$ differences at 55-75°N, 1250-1500 K during Feb-Mar. This reversal of the QBO signal between early and late winter is largely due to a reduction of $\overline{P}_\phi$ in the extratropical upper stratosphere under wQBO (Fig. 3d vs 3c). Reduction of $\overline{P}_{\phi}$ in these regions is most likely due to increased poleward RWB (Hitchman and Huesmann, 2007).

Positive QBO differences in $\overline{P}_{\phi}$ are found in the subtropical lower stratosphere near the eQBO-zero-wind line (Fig. 3e, f). These positive differences indicate enhanced PV gradients under eQBO and appear in both early and late winters. Similar effect can also been seen in the middle to upper stratosphereat 15-30°N, ~850-1250 K during wQBO (Fig. 3c-d) but the magnitude is noticeably smaller than its lower-level counterparts under eQBO. In the QBO difference plots (Fig. 3e, f), these upper-level effects under wQBO is overpowered by those associated with eQBO. In the region of large baroclinicity at 20-40°N, 400-550 K, $\overline{P}_{\phi}$ is larger during eQBO but smaller during wQBO. More positive $\overline{P}_{\phi}$ there under eQBO means that PRWs are able to propagate through the region into the middle to upper stratosphere.

Fig. 3 also shows that $\overline{P}_{\phi}$ near the equator becomes larger when the tropical winds are westerly but smaller when tropical winds are easterly. These QBO-related anomalies and those in the subtropical summer hemisphere are associated with barotropic instability of the subtropical easterly jet in the summer hemisphere, which occurs when the tropical winds are westerly (Hitchman *et al.*, 1987). The unstable RWs generated via barotropic instability is further amplified by inertial instability near the equator (O'Sullivan and Hitchman, 1992). Breaking of these unstable waves acts to sharpen PV gradients at the equator (Hitchman and Huesmann, 2007), thus the rather large values of $\overline{P}_{\phi}$ at 10°S-10°N (Fig. 3a-d). These low-latitude QBO-signals display little seasonal variation.

We next examine RWB by showing the seasonal progression of the zonally-averaged frequency of the overturning PV gradient $\overline{\gamma}$ during eQBO and wQBO winters and the associated QBO composite differences from November to March (Fig. 4). $\overline{\gamma}$ is in general inversely proportional to $\overline{P}_{\phi}$, thus, opposite in sign to those shown in Fig. 3. This inverse relationship is due to dynamics, i.e.

high PV gradients promote wave propagation (and hence less RWB) while mixing induced by RWB acts to smooth the background PV contours.

[[Insert Fig. 4 here]]

The key climatological features of $\bar{\gamma}$ are marked by regions with infrequent overturning of PV contours near the westerly jet core (i.e. the dotted lines in the extratropics) and at the equator, separated by a region with relatively large values of $\bar{\gamma}$ at 20-45°N (Fig. 4a-j). This region with noticeably more frequent reversals of PV contours (~10-15 days per month) signifies the so-called "surf zone". Frequent reversals of PV contours are also found in the subtropical summer stratosphere, reflecting barotropic instability of the subtropical easterly jet (Hitchman *et al*., 1987).

The differences in RWB between the two QBO phases in the extratropical winter hemisphere can be best appreciated by examining the seasonal evolution of the surf zone alongside with the polar vortex. During eQBO winters (Fig. 4a-e), the mid-latitude surf zone is mostly upright at 400-1000 K. $\bar{\gamma}$ at high latitudes at 60-70°N does not show strong seasonal variation from December through March either (Fig. 4b-e). Also, $\bar{\gamma}$ typically takes values ranging between 8 to 10 days per months near the polar vortex edge, which is not much smaller than those found in the surf zone. Fig. 4a-e thus suggests that RWB in the middle to upper stratosphereduring eQBO winters does not involve a gradual sharpening of PV gradients near the polar vortex edge.

In contrast, under wQBO, the surf zone in the middle to upper stratosphereis vertically connected with the surf zone in the lower stratosphere (Fig. 4f-j). The surf zone as a whole tilts equatorward with height in early winter (Fig. 4f-g), becomes upright in January (Fig. 4h), then tilts towards the North Pole in late winter (Fig. 4i-j). In addition, $\bar{\gamma}$ near the polar vortex edge gradually increases from under 4 days per month in November to over 12 days per month in March (Fig. 4f-j). These results suggest that RWB-related mixing is confined to the surf zone in the early winter but gradually works its way poleward in late winter. Fig. 4k-o shows that a sign reversal of the $\bar{\gamma}$

differences between the two QBO phases occurs around February, coinciding with the reversal of the HTE in the upper stratosphere in late winter (see Figs. 1f and 2b).

The QBO signal in the subtropical upper stratosphere of the NH is most strong in early winter (Fig. 4k-l). This is due to a northward and downward shift of the PRW absorption region during wQBO (Fig. 7b, e vs 7a, d). In November, the region with relatively large values of $\overline{\gamma}$ is located at 5-20°N, 1000-1500 K during eQBO (Fig. 4a) but become more poleward and downward at 20-40°N, 850-1250 K under wQBO (Fig. 4f). The negative $\overline{\gamma}$ differences centred at 25°N, 1250 K persist from November to February due to more frequent RWB in the surf zone under wQBO (Fig. 4k-o). The positive differences centred at 10°N, 1500 K are paired with negative differences at centred at 5°S, 1500 K, indicating a southward shift of the wave absorption during wQBO or northward shift of the wave absorption region during eQBO. These effects disappear since December, indicating that wave absorption at the low-latitude stratopause is affected by the QBO only in early winter.

Negative QBO differences in $\overline{\gamma}$ are also found in the lower stratosphere at 15-40°N, 400-550 K, which show little evidence of poleward migration or seasonal variation (Fig. 4k-o). The positive $\overline{\gamma}$ differences in the subtropical summer hemisphere in Fig. 4k-o are associated with the barotropic instability of the easterly jet due to the relocated zero-wind line by the QBO (O'Sullivan and Hitchman, 1992; HH09).

To better understand the QBO modulation of RWB in the middle to upper stratosphere, Fig. 5 shows scatterplots of PV gradient $\overline{P}_{\phi}$ vs $\overline{\gamma}$ in the mid- to upper stratospheric surf zone, i.e. 25-40°N, 850-1250 K for 2-month over-lapping running averages from October to January. As we expect, $\overline{P}_{\phi}$ (i.e. the strength of the waveguide) and $\overline{\gamma}$ (i.e. the frequency of RWB) are anti-correlated, which is consistent with the dissipative effect of RWB. However, $\overline{\gamma}$ is noticeably larger under wQBO than eQBO for a given value of $\overline{P}_{\phi}$. Such enhancement is most strong in early winter (i.e. Oct – Nov, Fig. 5a-b), during which the correlation between $\overline{\gamma}$ and $\overline{P}_{\phi}$ is statistically significant under wQBO (r = –0.71, $p \leq 0.05$) but fails to pass the statistical test under eQBO (r = –0.37, p = 0.23). These results confirm enhanced RWB under wQBO in the middle to upper stratospherewith strong mixing in the mid-latitude surf zone in early to middle winter.

[[Insert Fig. 5 here]]

3.2. Changes in wave mean-flow interaction

In this section, we examine the QBO modulation of wave-driving based on the EP fluxes and the density-weighted eddy PV fluxes Π. Previous studies have suggested that the HTE involves changes in PRWs as well as SRWs (e.g. Garfinkel *et al.*, 2012; White *et al.*, 2016). To examine their relative contributions, the analysis of Fig. 6 is repeated but separately for zonal wavenumber 1 (wave-1), zonal wavenumbers 2-3 (wave-2-3) and for zonal wavenumbers 5-10 (SRWs). These wave forcing analyses are performed for Nov-Dec and Feb-Mar, in order to highlight the early and late winter differences.

Fig. 6a-b shows the early and late winter climatology of the EP fluxes (arrows) and the density-weighted eddy PV flux $\Pi = \bar{\sigma}\overline{\hat{v}\hat{P}}^{*}$ (contours); the latter is equivalent to the EP flux divergence $(a\cos\phi)^{-1}\nabla\cdot\mathbf{F}$. The climatology of PRW propagation throughout the winter stratosphere is marked by upward pointing and equatorward tilted EP flux vectors (see Fig. 3a-d). Π is mostly negative (i.e. the converging EP fluxes) and centred at the polar vortex edge. The few small regions with positive Π near the equator and on the poleward flank of the westerly jets indicate internal wave generation, most likely due to localized instability (e.g. Simmons and Hoskins, 1978).

[[Insert Fig. 6 here]]

The early winter QBO signal in Π (Fig. 6c, coloured contours) is characterized by convergent EP flux anomalies at high-latitudes, i.e. negative Π differences poleward of 50°N and in the subtropical lower stratosphere at 20-40°N, 400-650 K. These Π anomalies are accompanied by enhanced upward EP flux vectors north of ~55°N and equatorward and poleward pointing EP flux vectors in the lower stratosphere. These EP flux anomalies indicate enhanced upward propagating and stronger wave forcing on the polar vortex, which is consistent with a weaker polar vortex in early winter during eQBO. Positive Π differences that are of relatively smaller amplitude are found at 20-45°N, 700-1250 K, where the mid- to upper stratospheric surf zone is located. The anomalous EP flux divergences there can be linked to RWB, which is enhanced during wQBO (Figs. 4 and 5).

In late winter, the wave forcing response at high-latitudes reverses the sign, i.e. larger values of Π near the polar vortex edge are found to associate with wQBO (Fig. 6d). The late-winter enhanced wave forcing under wQBO is again consistent with enhanced RWB in the middle to upper stratosphere; an effect that gradually expands from the surf zone into the high latitudes (see Fig. 4f-j), corresponding to a weaker polar vortex during Feb-Mar during wQBO winters (Figs. 1f and 2b).

In the subtropics, the QBO signal in Π is marked by negative differences in the lower stratosphere and positive difference in the middle to upper stratosphere. These subtropical QBO signals are present in both early and late winter in association with the QBO-zero wind lines. These QBO signals are accompanied by enhanced equatorward or poleward EP flux vectors in response to more positive or negative $\overline{P}_\phi$ northward of the corresponding QBO-zero-wind lines (Fig. 3e, f).

QBO modulation of wave forcing is separately into three bands of zonal wavenumbers and the Nov-Dec averages are shown in Fig. 7 while those for Feb-Mar averages are shown in Fig. 8. It is evident that the QBO modulation of Π is dominated by PRWs while SRWs play a relatively minor role, except near the SWJ where the EP flux vectors are noticeably large. Several regions of positive Π are featured and include the effects from both PRWs and SRWs, implying that instability and/or nonlinear wave-wave interactions might be involved. The exact role of nonlinearity is however complex and cannot be properly studied using seasonal averages or the zonal mean fields. It is thus beyond the scope of this paper but will be a subject of future studies.

[[Insert Figs. 7 and 8 here]]

Figs. 7 and 8 nevertheless suggests a complex interplay among wave-1, wave-2-3 and SRWs. In early winter, a weaker polar vortex during eQBO is largely due to enhanced wave-1 forcing in the middle to upper stratosphere (~700 K and above), where these waves are guided upward along the polar vortex edge (Fig. 7a-c). There is ~25% increase in wave-1 forcing during eQBO in comparison to those during wQBO. These upward wave-1 EP fluxes correspond to a northward shift of the critical line, thus consistent with the classic HT mechanism. The convergent differences of wave-2-3 in the lower stratosphere at 60-80°N, 400-650 K also contribute to enhanced PRW forcing on the polar vortex. The convergent differences of wave-2-3 at 60-80°N, 400-650 K are accompanied by anomalous equatorward and poleward pointing EP flux vectors and convergent differences in the subtropics (Fig. 7d-f), indicating enhanced RWB in the lower stratosphere under eQBO.

Divergent differences of wave-2-3 are however found at 20-50°N, 850-1250 K with meridional EP fluxes vectors that point equatorward and poleward near the surf zone (Fig. 7f). They are due to enhanced RWB during wQBO that is marked by more frequent overturning PV contours (Fig. 4f-g) and enhanced PV gradients near the polar vortex edge (Fig. 3c). Their magnitude is smaller than those associated with wave-1 under eQBO (1.8 m s^{-1} day^{-1} versus 2.8 ms^{-1} day^{-1}). The downward pointing EP fluxes at 45-65°N in the stratosphere indicate that upward propagating wave-2-3 is enhanced during wQBO in early winter.

SRWs are generated on the equatorward flank of the polar vortex and dissipate sideways in the middle to upper stratosphere at 700-1500 K during both eQBO and wQBO (Fig. 7g, h). This effect is significantly stronger and deeper in altitude during wQBO. The QBO signal there thus is marked by convergent differences at 35-45°N and divergent differences near the zero-wind lines and at 55-65°N (Fig. 7i).

Using a single-layer barotropic model, Scott (2019) recently studied meridional wave transfer between two waveguides in the winter stratosphere. It was found that the latitudinal separation between the high- and low-latitude waveguides is effectively reduced locally due to finite amplitude wave disturbances. Also, nonlinear transfer of wave activity from wave-2 to SRWs is noticeably enhanced when the low-latitude waveguide is located in the winter hemisphere. Fig. 7d-i confirms that this nonlinear effect becomes stronger in the middle to upper stratosphere during wQBO winters when the zero-wind line there is shifted into the winter hemisphere.

In late winter, the convergent wave-1 differences remain but become more confined to the high latitudes at 65-85°N, 350-1250 K (Fig. 8a-c). During eQBO, convergence of wave-1 is most strong in the upper stratosphere poleward 35°N (Fig. 8a). During wQBO, the region with large negative Π becomes more centred at the polar vortex edge and extends downward in the lower stratosphere (Fig. 8b). The latitudinally alternating negative, positive and negative wave -1 Π differences are merely due to a poleward and downward shift of the region with largest wave-1 forcing during wQBO.

The QBO signal in late winter wave-2-3 forcing is marked by the positive Π differences on both flanks of the polar vortex at 20-55°N, 850-1500 K and at 60-80°N, 350-1000 K (Fig. 8f). The absolute values of Π associated with wave-2-3 in these regions during wQBO is near twice as large as those under eQBO (Fig. 8e vs Fig. 8d). The positive differences in between are due to an equatorward shift of the region of wave-2-3 generation. The combined effect of wave-1 and wave-2-3 leads to weaker (stronger) net PRW convergence in the extratropical winter stratosphere during eQBO (wQBO) (Fig. 6d).

From Figs. 6-8, we conclude that enhanced upward propagating wave-1 and their absorption near the polar vortex in the middle to upper stratosphere play a dominant role in causing a weaker polar vortex under eQBO while convergent anomalies of wave-2-3 in the lower stratosphere contribute to an overall enhanced wave forcing. A build-up effect of RWB in the middle to upper stratosphere that involves nonlinear meridional wave transfer and a gradual enhancement of wave-2-3 forcing on the flanks of the polar vortex edge is responsible for the late winter weakening of the polar vortex during wQBO. In addition to the differences in seasonal development and latitude/height locations, QBO modulation of wave absorption and/or RWB are wavenumber dependent. The vertical component of the EP fluxes F_z at 100 hPa alone is thus insufficient in explaining the HTE.

To further demonstrate the key difference between the two QBO phases in terms of the polar vortex response to wave driving, Fig. 9a shows scatter plots of Nov-Jan mean vertical component of the EP fluxes $F^{(\theta)}$ in the lower stratosphere at 45-85°N, 350-450 K and the zonal-mean wind $\bar{u}$ averaged along the entire polar vortex edge at 45-75°N, 450-1500 K averaged for the same months. It is evident that $F^{(\theta)}$ and $\bar{u}$ are anti-correlated ($r = -0.72$, $p < 0.05$), consistent with the notion that stronger wave forcing from the lower stratosphere leads to a weaker polar vortex.

[[Insert Fig. 9 here]]

The cumulative effect of RWB can be appreciated by relating the strength of the polar vortex with the EP fluxes $F^{(\theta)}$ in an earlier period, which is shown in Fig. 9b. In this case, $F^{(\theta)}$ is averaged over Oct-Dec while $\bar{u}$ remains as the Nov-Jan average so that the upward wave fluxes in the lower stratosphere lead the zonal-mean zonal wind by one month. Without separating the data into eQBO and wQBO phases, $F^{(\theta)}$ and $\bar{u}$ remain anti-correlated ($r = -0.73$, $p < 0.05$). Thus, as far as the total wave forcing is concerned there is hardly any difference between Fig. 9a and Fig. 9b.

However, differences become obvious if the correlations are examined separately for the two QBO phases. In Fig. 9a, the relationship between $F^{(\theta)}$ and $\bar{u}$ is stronger for the eQBO subgroup ($r = -0.85$) than for the wQBO subgroup ($r = -0.64$), while for Fig. 9b, the opposite holds and the correlation becomes much stronger for wQBO ($r = -0.83$) but not statistically significant for eQBO ($r = -0.46$, $p = 0.15$). This suggests that the polar vortex response to the wave fluxes from below involves successive RWB events during wQBO winters in contrast to the within season response dominates during eQBO winters. Weaker but similar responses can also be seen for the Feb-Mar averages (Fig. 9c-d). Also, larger values of $\overline{u}$ becomes to be associated with eQBO rather than wQBO. Such a reversal would become more pronounced if the extratropical $\overline{u}$ is avaraged above 850 K (not shown).

3.3. Down-gradient eddy PV fluxes

RWB-related eddy PV fluxes are typically directed down the background PV gradients in the winter stratosphere (see Sec. 2.1). We expect this effect to be more pronounced in the surf zone under wQBO. In this section, we focus on the Nov-Jan period to demonstrate such an effect.

Fig. 10a shows the climatology of down-gradient eddy PV flux Γ averaged over Nov-Jan when all wavenumbers are included. As expected, Γ is predominately negative in the extratropical winter stratosphere, except for a few small regions on the poleward flank of the tropospheric subtropical jet and in the polar stratosphere where either instability, nonlinear wave-wave interaction or upscaling of SRWs play a role (e.g. Birner *et al.*, 2013).

[[Insert Fig. 10 here]]

The corresponding QBO differences in Γ are shown in Fig. 10b, c. The responses are averaged over the overlapping running two-month periods of Nov-Dec and Dec-Jan so that we can examine the transition of RWB. It is evident that the extratropical QBO signal in Γ is mostly confined to the vicinity of the polar vortex edge. During Nov-Dec, the QBO signal is characterized by negative differences on the poleward flank of the polar vortex and positive differences on its equatorward flank (Fig. 10b). The negative Γ differences poleward of 55°N indicate enhanced down-gradient eddy PV fluxes during eQBO, corresponding to the enhanced wave-1 forcing in the same region (Fig. 7c). The positive Γ differences at 35-55°N, 850-1500 K (Fig. 10b) are associated with enhanced RWB under wQBO, which is marked by enhanced over turning of the PV contours in the mid-latitude surf zone (Fig. 4k, l).

In Dec-Jan, the positive Γ differences intensify and extend downward into the lower stratosphere while those negative differences of Γ at high latitudes disappear and are replaced by positive Γ differences (Fig. 10c). Positive Γ differences are also found in the subtropics and polar stratosphere, due to more wave activity being steered latitudinally towards both lower and higher latitudes during wQBO. The enhanced wave activity in extratropical winter stratosphere is however accompanied by a stable polar vortex (Fig. 1c). Such a combination typically occurs during the early stage of RWB (McIntyre, 1982). A further enhancement of Γ on both flanks of the polar vortex can be obtained during wQBO in Feb-Mar averages if the analysis is restricted to the zonal wavenubers 2 to 3 (not shown), corresponding to a weaker than average polar vortex in late winter under wQBO (Fig. 1f).

Enhanced wave activity is also found near the zero-wind line that is shifted into the NH and these low-latitude effects resemble those in Fig. 3e. These low-latitude effects are consistent with QBO modulation of wave reflection and/or meridional transfer of wave activity from low zonal wavenumber to higher zonal wavenumbers (Watson and Gray, 2014; Scott, 2019).

3.4. The role of the QBO-MMC

To understand how the QBO-MMC may be linked to the HTE, Fig. 11 shows meridional velocity $\overline{v}$ over the latitude-height cross section of 30°S-40°N and 400-1500 K during November for eQBO and wQBO averages and corresponding QBO differences. The QBO-MMC with its NH divisions is indicated by the blue arrows in Fig. 11a-b, which is aligned with the positions of the maxima and minima QBO-related $\overline{v}$ differences below 1000 K (Fig. 11c). The northward circulation in the subtropical NH (i.e. 5-25°N) is enhanced at ~600 K (50 hPa) under eQBO but at ~400 K (100 hPa) and ~850 K (10 hPa) under wQBO. The QBO-MMC is also asymmetric about the equator, being stronger in the winter hemisphere but weaker in the summer hemisphere. These features are consistent with both the theory and the observed QBO-MMC (Plumb and Bell, 1982; Kinnersley, 1999). Similar results can be obtained for other winter months (not shown).

[[Insert Fig. 11 here]]

The QBO-MMC can be linked to the results presented in previous sections. Namely, PV gradients are found to be enhanced in the subtropical layers where the QBO-MMC is directed poleward (Figs. 3). RWs are also preferably guided equatorward in the same layers where the QBO-MMC is directed poleward where PV gradients are enhanced (Fig. 6). These effects are found to be further accompanied by enhanced RWB in the same level because the equatorial propagating RWs would result in poleward wave reflection due to a northward shift of the zero-wind line at the same height region (Killworth and McIntyre, 1985; Watson and Gray, 2014). We thus suggest that the combined effect of the QBO-MMC and the zero-wind line is responsible for the enhanced RWB in the lower stratosphere during eQBO winters. In the context of the HTE, the RWB in the lower stratosphere involves the following positive feedbacks. Namely: the QBO-MMC-induced PV gradients → enhanced equatorward propagation of PRWs → stronger poleward wave reflection due to non-linear critical layer → more frequent generation and breaking of SRWs near the SWJ → more positive PV gradients at 20-40°N → more PRWs entering the stratosphere.

Our interpretation of the QBO-MMC in altering the waveguide and RW propagation in the subtropical lower stratosphere is in agreement with previous studies. For instance, Hitchman and Leovy (1986) analysed the daily mapped fields from the Nimbus 7 Limb Infrared Monitor of the Stratosphere (LIMS) for the period of October, 1978 to May, 1979 and found that meridional PV gradients are enhanced in a subtropical layer where the QBO-MMC was directed poleward. Using idealized model simulations in which the zonal winds in the equatorial lower stratosphere were constantly easterly, Norton (1994) found that PV gradients are enhanced on the equatorward flank of the surf zone with a poleward expansion of the affected region. It has also been found that the northward flow of the QBO-MMC at ~600 K (50 hPa) during eQBO winters interacts with PRWs whereby it contributes to an overall enhanced residual-mean meridional circulation in the extratropical lower stratosphere (Garfinkel *et al.*, 2012; Lu *et al.*, 2014; White *et al.*, 2015).

Apart from the QBO-MMC, the largest QBO signal in $\overline{v}$ (up to –0.7 m s^{-1}) is in fact found in the subtropical middle to upper stratosphere at ~850-1250 K where the cross-equatorial flow is climatologically strong (Fig. 11). It shows that the northward flow is enhanced at the isentropic layers of 850-1250 K in the subtropical NH during wQBO but it is located near the equator and at higher altitudes at ~1500 K and above during eQBO (Fig. 11a, b). Thus, there is northward and downward shift of the region of critical-layer wave absorption during wQBO.

The cross-equatorial flow near the stratopause is known to be most sensitive to wave driving of the winter stratosphere (Semeniuk and Shepherd, 2001). It is further affected by the semi-annual oscillation (SAO), a dominant feature in tropical upper stratosphere winds (Smith *et al*., 2017). An anomalous downward and poleward motion in the equatorial upper stratosphere appears when the SAO is in its westerly phase (wSAO) because the westerly SAO (wSAO) descends much faster than the average equatorial winds (Hitchman and Leovy, 1986). This wSAO-MMC in the NH is indicated by the purple circle with arrows in Fig. 11b. Although the wSAO is largely driven by Kelvin and gravity waves, it tends to have a larger amplitude and becomes more persistent when the lower stratospheric QBO is in its westerly phase (Smith *et al*., 2017). This coupling between the wQBO and wSAO is most pronounced in early winter around November (Smith *et al*., 2017).

In early winter, the northward flow of wQBO-MMC at ~850 K is complemented by the same effect at the isentropic layers of 1000-1250 K associated with the wSAO-MMC (Fig. 11b). Wave mean-flow interaction is enhanced at those isentropic layers where PV gradients in the subtropics are enhanced (Figs. 6c, 7f and 3c). As PRWs are preferably guided towards to equator at 850-1250 K, the extratropical westerly winds above 1250 K would become less disturbed due to the reduced upward wave activity. The enhanced upper-level westerly winds would then result in further equatorward refraction of PRWs below at 850-1250 K because PRWs can only propagate through a region where the background flow is weakly westerly ($\leq$ 50 m s^{-1}) (Charney and Drazin 1961). We expect this feedback to be most pronounced in early winter because the radiative-driven upper-level polar vortex is climatologically strong during the time (Andrew *et al*., 1987). Because the SAO in the upper stratosphere is typically in its westerly phase during September to November but switches to its easterly phase since mid- December. The contribution from the SAO-MMC is most pronounced in early winter. Together with the northward shifted zero-wind line there, RWB is enhanced in the middle to upper stratosphere during wQBO due to increased wave activity and the reduced meridional extent between the polar vortex and the zero-wind line (Scott, 2019).

4. Conclusions and Discussion

Motivated by the observed intra-seasonal dependence in the HTE, this tropical-extratropical connection is re-examined here by focusing on QBO modulation of RWB. Based on the NCEP-CFS reanalysis data sets in isentropic coordinates that covers the 1979 – 2017 period, we have studied QBO-related changes in RWB alongside with zonal-mean circulation, the QBO-MMC and wave-number-dependent wave forcing on the mean flow. Our results suggest RWB is generally enhanced in the height region where the QBO zero-wind line is shifted into the NH. The height-levels where RWB is most enhanced appear to be linked to the poleward flow induced by the QBO-MMC and the SAO-MMC. The classic mechanism proposed for the HTE whereby QBO-induced changes in the total volume or width of stratospheric waveguide regulates the net wave forcing on the polar vortex nevertheless remains valid. It is further supplemented by additional effects that involve RWB: 1) the enhanced RWB and waveguide in the subtropical lower stratosphere during eQBO winters that allows more PRWs to enter the stratosphere; 2) a persistent and cumulative effect of RWB in the middle to upper stratosphere during wQBO winters. The latter is responsible for the observed intra-seasonal variation of the HTE.

RWB acts to reshape the background waveguide and alter the structure of the waves via nonlinear wave transfer (Waugh and Dritschel, 1999; Scott, 2019). The characteristics of RWB and the polar vortex responses differ distinctly from eQBO and wQBO winters. Fig. 12 depicts a schematic diagram that highlights our key findings. During eQBO winters, an increase in upward propagating wave-1 and the subsequent absorption by the background mean flow in the mid- to high latitudes play a predominant role in disturbing the polar vortex. RWB is also enhanced in the subtropical lower stratosphere where PV gradients are climatologically small (Fig. 12a, b). RWB acts to strengthen the background PV gradients, allowing more PRWs to enter the stratosphere at 20-40°N (Figs. 3a-b and 6c). Poleward refraction of PRWs from the RWB region also leads to enhanced EP flux convergence of wave-2-3 at high latitudes, further contributing to enhanced wave forcing on the polar vortex. These eQBO-related wave absorption and RWB anomalies involve very little seasonal variation. Thus, a SSW event, or a disturbed vortex, may occur at any point during the winter season.

[[Insert Fig. 12 here]]

During wQBO winters, RWB is enhanced in the middle to upper stratosphere and the effect is dominated by wave-2-3 (Figs. 12c, d and 7f, 8f). In early winter, RWB acts to sharpen PV gradients on the equatorial flank of the polar vortex while frequent overturning of PV contours occurs in the surf zone at 20-45°N, 850-1000 K (Figs. 12c and 4c, e). The down-gradient wave activity into the surf zone is accompanied by reduced wave activity at high latitudes, thus a less disturbed polar vortex in early winter during wQBO (Fig. 12c). As the winter progresses, RWB gradually "erodes" the polar vortex and the surf zone expands poleward. The poleward confinement of wave activity tightens PV gradients at the vortex edge, weakening the polar vortex (Fig. 12d). Thus, SSWs are more likely to occur in late winter during wQBO winters as it requires "pre-conditioning" by successive RWB events. Because its effect on the polar vortex switches from reinforcement to disturbance around February, examining the HTE solely based on mid-winter averages can be somehow misleading.

According to idealized model simulations, RWB is intrinsically nonlinear and sensitive to both background flow and the structure of wave forcing from below (Waugh and Dritschel, 1999; Polvani and Saravanan, 2000; Scott and Dritschel, 2005; Scott, 2019). Given the relatively short period under consideration (i.e. 1979-2017), uncertainties are expected in the reported QBO signal especially the magnitude and the timing of late winter reversal. The QBO signals may also liaise with other processes, including solar forcing, snow cover and ENSO. For instance, El Nino events occurred more often when the QBO was in its westerly phase in recent decades; this may partially contributed to a weaker-than-expected ENSO effect on the stratospheric polar vortex (Domeisen *et al.*, 2019). Likewise, such an alias may alter the seasonal development of RWB and the polar vortex responses to the QBO, manifesting by the observed decadal or multi-decadal variation of the HTE (Gray *et al.*, 2004; Lu *et al.*, 2008; 2014).

Considerable progress has been made in reproducing the QBO itself in more comprehensive climate models recently via improved parametrization of small-scale waves with increased vertical resolution (Geller *et al.*, 2016, Butchart *et al.*, 2018). But replicating the HTE with the observed strength remains a challenge (Garfinkel *et al.*, 2018). A faithful reproduction of the HTE in model simulations may require good representations of both the QBO in the lower to middle stratosphere and the SAO in the upper stratosphere and lower mesosphere, which remains a challenge due to the difficulties of resolving/parameterizing the small-scale gravity waves associating with tropical convection (Geller *et al.*, 2016; Osprey *et al.*, 2018).

Acknowledgements: This study is part of the British Antarctic Survey (BAS) Polar Science for Planet Earth programme and the National Centre for Atmospheric Science (NCAS) of the Natural Environment Research Council (NERC). HL, LJG and SO were supported by the NERC North Atlantic Climate System Integrated Study (ACSIS) (NE/N018028). SO and LJG were also partially supported by the NERC grant NE/P006779/1. MHH was supported by the National Science Foundation grant AGS-1555851. We acknowledge use NCEP CFSR reanalysis data on isentropic coordinates (https://www.ncdc.noaa.gov/data-access/)

References:

Abatzoglou, J.T. and Magnusdottir G. (2007). Wave breaking along the stratospheric polar vortex as seen in ERA-40 data. *Geophys. Res. Lett*., 34, L08812.

Albers, J.R. and Birner, T. (2014). Vortex preconditioning due to planetary and gravity waves prior to stratospheric sudden warmings. *J. Atmos. Sci.,* 71, 4028–4054.

Andrews, D.G., Holton, J.R. and Leovy, C.B. (1987). Middle Atmosphere Dynamics. Academic Press, Cambridge, MA.

Andrews, M.B., Knight, J.R., Scaife, A.A., Lu, Y., Wu, T., Gray, L.J., & Schenzinger, V. (2019). Observed and simulated teleconnections between the stratospheric Quasi-Biennial Oscillation and Northern Hemisphere winter atmospheric circulation. *J. Geophys. Res*., 124, 1219–1232.

Anstey, A. and Shepherd, T.G. (2014). High-latitude influence of the quasi-biennial oscillation. *Quart. J. Roy. Meteor. Soc*., 140, 1–21.

Baldwin, M.P., *et al.* (2001). The quasi-biennial oscillation. *Rev. Geophys*., 39(2), 179–229.

Baldwin, M.P. and Dunkerton, T.J. (1999). Propagation of the Arctic Oscillation from the stratosphere to the troposphere. *J. Geophys. Res*. 104, 30937–30946.

Birner, T., Thompson, D.W. J. and Shepherd, T.G. (2013). Up-gradient eddy fluxes of potential vorticity near the subtropical jet. *Geophys. Res. Lett.*, 40, 5988-5993.

Butchart, N. *et al.* (2018). Overview of experiment design and comparison of models participating in phase 1 of the SPARC Quasi-Biennial Oscillation initiative (QBOi), *Geosci. Model Dev*., 11, 1009-1032.

Calvo, N., Giorgetta, M.A. and Peña‐Ortiz, C. (2007). Sensitivity of the boreal winter circulation in the middle atmosphere to the quasi‐biennial oscillation in MAECHAM5 simulations, *J. Geophys. Res.*, 112, D10124.

Charney, J.G. and Drazin, P. G. (1961). Propagation of planetary-scale disturbances from the lower into the upper atmosphere, *J. Geophys. Res*., 66(1), 83-109, doi:10.1029/JZ066i001p00083.

Cohen, J., and D. Entekhabi (1999). Eurasian snow cover variability and northern hemisphere climate predictability, *Geophys. Res. Lett*., 26(3), 345–348, doi:10.1029/1998GL900321.

Domeisen, D.I., Garfinkel, C.I. and Butler, A.H. (2019). The teleconnection of El Niño Southern Oscillation to the stratosphere. *Rev. Geophys*, 57, 5– 47.

Dunkerton, T.J. and Baldwin, M.P. (1991). Quasi-biennial modulation of planetary-wave fluxes in the Northern Hemisphere winter. *J. Atmos. Sci*., 48, 1043-1061.

FUB (2017). Freie Universität Berlin: The Quasi-Biennial-Oscillation (QBO). Data Series. http://www.geo.fu-berlin.de/en/met/ag/strat/produkte/qbo/. Accessed: 2017-07-11.

Garfinkel, C.I. and D.L. Hartmann, 2011: The influence of the Quasi-Biennial Oscillation on the troposphere in winter in a hierarchy of models. Part II: Perpetual winter WACCM runs. *J. Atmos. Sci*., 68, 2026–2041.

Garfinkel, C.I., Schwartz, C., Domeisen, D.I.V., Son, S.-W., Butler, A.H. and White, I.P. (2018). Extratropical atmospheric predictability from the quasi-biennial oscillation in subseasonal forecast models. *J. Geophys. Res.* 123, 7855–7866.

Garfinkel, C.I., Shaw, T.A., Hartmann, D.L. and Waugh, D.W. (2012). Does the Holton-Tan mechanism explain how the quasi-biennial oscillation modulates the Arctic polar vortex? *J. Atmos. Sci*., 69, 1713-1733.

Geller, M.A. *et al.* (2016). Modeling the QBO: Improvements resulting from higher model vertical resolution. *J. Adv. Model. Earth Syst.*, 8, 1092–1105.

Gray, L.J., Anstey, J.A., Kawatani, Y., Lu, H., Osprey, S. and Schenzinger, V. (2018). Surface impacts of the Quasi Biennial Oscillation. *Atmos. Chem. Phys*., 18, 8227-8247.

Gray, L.J., Crooks, S., Pascoe, C., Sparrow, S. and Palmer, M. (2004). Solar and QBO influences on the timing of stratospheric sudden warmings. *J. Atmos. Sci.,* 61, 2777–2796.

Gray, L.J. *et al.* (2010). Solar influence on climate. *Rev. Geophys.*, 48, RG4001, doi:10.1029/2009RG000282.

Gray, L.J., Sparrow, S., Juckes, M., O'Neill, A. and Andrews, D.G. (2003). Flow regimes in the winter stratosphere of the northern hemisphere. *Quart. J. Roy. Meteor. Soc.*, 129, 925-945.

Greer, K., Thayer, J.P. and Harvey, V.L. (2013). A climatology of polar winter stratopause warmings and associated planetary wave breaking. *J. Geophys. Res. Atmos*., 118, 4168–4180.

Hitchman, M.H. and Huesmann, A.S. (2007). A seasonal climatology of Rossby wave breaking in the layer 330-2000 K. *J. Atmos. Sci.*, 64, 1922-1940.

Hitchman, M.H. and Huesmann, A.S. (2009). Seasonal influence of the quasi-biennial oscillation on stratospheric jets and Rossby wave breaking. *J. Atmos. Sci.*, 66, 935-946.

Hitchman, M.H., Gille, J.C. and Bailey, P.L. (1987). Quasi-stationary, zonally asymmetric circulations in the equatorial lower mesosphere. *J. Atmos. Sci*., 44, 2219–2236.

Hitchman, M.H. and Leovy, C.B. (1986). Evolution of the zonal mean state in the equatorial middle atmosphere during October 1978–May 1979. *J. Atmos. Sci*., 43, 3159–3176.

Holton, J.R. and Tan, H.C. (1980). The influence of the equatorial quasi-biennial oscillation on the global circulation at 50mb. *J. Atmos. Sci.*, 37, 2200-2208.

Holton, J.R. and Tan, H.C. (1982). The quasi-biennial oscillation in the Northern Hemisphere lower stratosphere. *J. Met. Soc. Japan*, 60, 140–148.

Hoskins, B.J., McIntyre, M.E. and Robertson, A.W. (1985). On the use and significance of isentropic potential vorticity maps. *Quart. J. Roy. Meteor. Soc.*, 111, 877-946.

Hu, Y. and Tung, K.K. (2002). Tropospheric and equatorial influences on planetary-wave amplitude in the stratosphere. *Geophys. Res. Lett*., 29(2), 1019.

Karoly, D. and Hoskins, B.J. (1982). Three-dimensional propagation of planetary waves. *J. Met. Soc. Japan,* 60, 109–123.

Kidston, J, Scaife, A.A., Hardiman, S.C., Mitchell, D.M., Butchart, N., Baldwin, M.P. and Gray, L.J. (2015). Stratospheric influence on tropospheric jet streams, storm tracks and surface weather. *Nat. Geo.*, 8(6), 433-440.

Killworth, P.D. and McIntyre, M.E. (1985). Do Rossby-wave critical layers absorb, reflect or over-reflect? *J. Fluid Mech*., 161, 449–462.

Kinnersley, J.S. (1999). Seasonal asymmetry of the low- and middle-latitude QBO circulation anomaly. *J. Atmos. Sci*., 56, 1140–1153.

Kodera, K. (1994). Influence of volcanic eruptions on the troposphere through stratospheric dynamical processes in the northern hemisphere winter, *J. Geophys. Res.*, 99(D1), 1273–1282.

Labe, Z., Peings, Y., and Magnusdottir, G. (2019). The effect of QBO phase on the atmospheric response to projected Arctic sea ice loss in early winter. *Geophys. Res. Lett.*, 46, 7663–7671.

Labitzke, K. (1982). On the interannual variability of the middle stratosphere during the Northern Winters. *Quart. J. Roy. Meteor. Soc.*, 60(1), 124–139.

Lait, L.R. (1994). An alternative form for potential vorticity. *J. Atmos. Sci.*, 51, 1754-1759.

Leovy, C.B., Sun, C.-R., Hitchman, M.H., Remsberg, E.E., Russell III, J.M., Gordley, L.L., Gille, J.C. and Lyjak, L.V. (1985). Transport of ozone in the middle stratosphere: Evidence for planetary wave breaking. *J. Atmos. Sci*., 42, 230–244.

Limpasuvan V., Thompson D. W. J., and Hartman D. L. (2004). The life cycle of the Northern Hemisphere sudden stratospheric warmings, *J. Clim.*, 17, 2584–2596.

Lu, H., Baldwin, M.P., Gray, L.J. and Jarvis, M.J. (2008). Decadal-scale changes in the effect of the QBO on the Northern stratospheric polar vortex. *J. Geophys. Res.*, 113, D10114.

Lu, H., Bracegirdle, T.J., Phillips, T., Bushell, A.B. and Gray, L.J. (2014). Mechanisms for the Holton-Tan relationship and its decadal variation. *J. Geophys. Res.*, 119, 2811-2830.

Lu, H., Gray, L.J., White, I.P. and Bracegirdle, T.J. (2017). Stratospheric response to the 11-yr solar cycle: Breaking planetary waves, internal reflection, and resonance. *J. Clim.,* 30, 7169–7190.

Marshall, A.G. and Scaife A.A. (2009). Impact of the QBO on surface winter climate. *J. Geophys. Res.*, 114, D18110.

Matsuno, T. (1970). Vertical propagation of stationary planetary waves in the winter Northern Hemisphere. *J. Atmos. Sci.*, 27, 871-883.

Matsuno, T. (1971). A dynamical model of the stratospheric sudden warming. *J. Atmos. Sci.,* 28, 1479–1494.

McIntyre, M.E. (1982). How well do we understand the dynamics of stratospheric warmings? *J. Meteor. Soc. Japan*, 60, 37–65.

McIntyre, M.E. and Palmer, T.N. (1983). Breaking planetary waves in the stratosphere. *Nature*, 305, 593-600.

McIntyre, M.E. and Palmer, T.N. (1984). The surf zone in the stratosphere. *J. Atmos. Terr. Phys*., 46(6), 825-849.

Naito, Y. and Yoden, S. (2006). Behavior of planetary waves before and after stratospheric sudden warming events in several phases of the equatorial QBO. *J. Atmos. Sci.*, 63, 1637–1649.

Nakamura, T., K. Yamazaki, K. Iwamoto, M. Honda, Y. Miyoshi, Y. Ogawa, Y. Tomikawa, and J. Ukita (2016). The stratospheric pathway for Arctic impacts on midlatitude climate, *Geophys. Res. Lett*., 43, 3494–3501, doi: 10.1002/2016GL068330.

Naoe, H. and Shibata, K. (2010). Equatorial quasi-biennial oscillation influence on northern winter extratropical circulation. *J. Geophys. Res*., 115, D19102.

Naujokat, B. (1986). An Update of the Observed Quasi-Biennial Oscillation of the stratospheric winds over the tropics. *J. Atmos. Sci*., 43(17), 1873-1877.

Norton, W.A. (1994). Breaking Rossby waves in a model stratosphere diagnosed by a vortex-following coordinate system and a technique for advecting material contours, *J. Atmos. Sci*., 51, 654–673.

Osprey, S., Geller, M. and Yoden, S. (2018). The stratosphere and its role in tropical teleconnections. *Eos*, 99, doi: 10.1029/2018EO097387.

O'Sullivan, D.J. and Hitchman, M.H. (1992). Inertial instability and Rossby wave breaking in a numerical model. *J. Atmos. Sci*., 49, 991–1002, doi: 10.1175/1520-0469.

O'Sullivan D.J. and Salby, M.L. (1990). Coupling of the quasi-biennial oscillation and the extratropical circulation in the stratosphere through planetary wave transport. *J. Atmos. Sci.* 47, 650–673.

O'Sullivan, D.J. and Young, R.E. (1992). Modeling the quasi-biennial oscillation's effect on the winter stratospheric circulation. *J. Atmos. Sci*., 49, 2437–2448, doi:10.1175/1520-0469.

Pascoe, C.L., Gray, L.J. and Scaife, A.A. (2006). A GCM study of the influence of equatorial winds on the timing of sudden stratospheric warmings. *Geophys. Res. Lett*.,33, L06825.

Peings, Y., Douville, H., Colin, J., Martin, D.S., & Magnusdottir, G. (2017). Snow-NAO teleconnection and its modulation by the Quasi-Biennial Oscillation. *J. Clim.*, 30, 10,211–10,235.

Plumb, R.A. and Bell, R.C. (1982). A model of the quasi-biennial oscillation on an equatorial beta-plane. *Quart. J. Roy. Meteor. Soc.*, 108, 335-352, doi:10.1002/qj.49710845604.

Polvani, L.M. and Saravanan, R.R. (2000). The three-dimensional structure of breaking Rossby waves in the polar wintertime stratosphere. *J. Atmos. Sci.,* 57, 3663–3685.

Robock, A. (2000). Volcanic eruptions and climate. *Rev. Geophys.*, 38, 191– 219.

Ruzmaikin, A., Feynman, J., Jiang, X. and Yung, Y.L. (2005). Extratropical signature of the quasi-biennial oscillation. *J. Geophys. Res.*, 110, D11111.

Saha, S. *et al.* (2012). *NCEP Climate Forecast System Version 2 (CFSv2). Daily Products*. Research Data Archive at the National Center for Atmospheric Research, Computational and Information Systems Laboratory. https://doi.org/10.5065/D69021ZF. Accessed 10/07/2017.

Scaife, A.A., Athanassiadou, M., Andrews, M., Arribas, A., Baldwin, M., Dunstone, N., Knight, J., MacLachlan, C., Manzini, E., Müller, W.A., Pohlmann, H., Smith, D., Stockdale, T., and Williams, A. (2014). Predictability of the quasi-biennial oscillation and its northern winter teleconnection on seasonal to decadal timescales, *Geophys. Res. Lett*., 41, 1752–1758.

Schenzinger, V., Osprey, S., Gray, L.J. and Butchart, N. (2017). Defining metrics of the Quasi-Biennial Oscillation in global climate models, *Geosci. Model Dev.,* 10, 2157-2168.

Scherhag, R. (1952). Die explosionsartige Stratosphärenerwärmung des Spätwinters 1951/1952. Deutscher Wetterdienst (US Zone) 6:51–63.

Schoeberl, M.R. and Smith, A.K. (1986). The integrated enstrophy budget of the winter stratosphere diagnosed from LIMS data. *J. Atmos. Sci.,* 43, 1074–1086.

Schoeberl, M.R., Lait, L.R., Newman, P.A. and Rosenfield, J.E. (1992). The structure of the polar vortex. *J. Geophys. Res*., 97(D8), 7859–7882.

Scott, R.K. (2019). Nonlinear latitudinal transfer of wave activity in the winter stratosphere. *Q J R Meteorol Soc*., 1 - 14 doi.org/10.1002/qj.3536.

Scott, R.K and Dritschel, D.G. (2005). Quasi-geostrophic vortices in compressible atmospheres. *J. Fluid Mech*., 530, 305-325.

Semeniuk, K. and Shepherd, T.G. (2001). Mechanisms for Tropical Upwelling in the Stratosphere. *J. Atmos. Sci.*, 58, 3097–3115.

Simmons, A.J. and Hoskins, B.J. (1978). The life cycles of some nonlinear baroclinic waves. *J. Atmos. Sci.*, 35, 414-432.

Smith, A.K., Garcia, R.R., Moss, A.C. and Mitchell, N.J. (2017). The semiannual oscillation of the tropical zonal wind in the middle atmosphere derived from satellite geopotential height retrievals. *J. Atmos. Sci.,* 74, 2413–2425.

Tung, K.K. (1979). A theory of stationary long waves. Part III: Quasi-normal modes in a singular waveguide. *Mon. Wea. Rev*., 107, 751–774.

Tung, K.K. (1986). Nongeostrophic theory of zonally averaged circulation. Part I: Formulation. *J. Atmos. Sci*., 43, 2600–2618.

Waugh, D.W. and Dritschel, D.G. (1999). The Dependence of Rossby wave breaking on the vertical structure of the polar vortex. *J. Atmos. Sci.,* 56, 2359–2375.

Watson, P.A. G. and Gray, L.J. (2014). How does the quasi-biennial oscillation affect the stratospheric polar vortex? *J. Atmos. Sci*., 71, 391-409.

White, I.P., Lu, H., Mitchell, N.J. and Phillips, T. (2015). Dynamical response to the QBO in the Northern Winter stratosphere: Signatures in wave forcing and eddy fluxes of potential vorticity. *J. Atmos. Sci*., 72, 4487–4507.

White, I.P., Lu, H. and Mitchell, N.J. (2016). Seasonal evolution of the QBO-induced wave forcing and circulation anomalies in the northern winter stratosphere. *J. Geophys. Res.*, 121, 10,411–10,431.

Yamashita, Y., Akiyoshi, H. and Takahashi, M. (2011). Dynamical response in the Northern Hemisphere midlatitude and high-latitude winter to the QBO simulated by CCSR/NIES CCM. *J. Geophys. Res.*, 116, D06118.

Figure Captions:

Fig. 1. (a, b): Zonal-mean zonal wind $\overline{u}$ during Nov-Jan and Feb-Mar for eQBO winter averages. Solid and dashed contours represent positive and negative winds with a contour interval of 5 m s^{-1}. The zero-wind line is marked by the thick-black line. (c, d): same as (a, b) except for wQBO winters. (e, f): corresponding QBO composite differences (eQBO–wQBO) with red and blue shadings representing westerly and easterly anomalies The thick solid and dashed lines near the equator indicate the zero-wind lines for wQBO and eQBO, respectively. The average location of the polar vortex edge is indicated by the dotted lines in (e, f). The cross-hatchings specify statistical significance at 95% levels.

Fig. 2. Climatology (lined contours with 5°K interval) and corresponding QBO composite differences (eQBO–wQBO) of the zonal-mean temperature $\overline{T}$ during Nov-Jan (a) and Feb-Mar (b).

Fig. 3. (a-d): Same as Fig. 1(a-d) except for zonal-mean meridional PV gradient $\overline{P}_{\phi}$ with a contour interval of 0.25 x 10^{-5} K m kg^{-1} s^{-1}. Following Lait (1994), $\overline{P}_{\phi}$ is multiplied by $(\theta/350)^{-9/2}$ to account for its exponential increase with height. (e,f): corresponding QBO composite difference (eQBO–wQBO) of $\overline{P}_{\phi}$ (colour shaded) with climatological $\overline{P}_{\phi}$ (grey contours). The eQBO and wQBO zero-wind lines (i.e. thick solid and dashed lines near the equator) and the average location of the polar vortex edge (grey dotted line) are shown. The cross-hatchings indicate statistical significance at 95% levels.

Fig. 4. (a-e): seasonal march (November to March) of the frequency of daily reversal of meridional PV gradients $\overline{\gamma}$ (in days per month) for eQBO winter mean. The contour interval is 2-days. (f-j): same as (a-e) except for wQBO mean. Regions with large values of $\overline{\gamma}$ are shaded in dark-grey to highlight the surf zone. (k-o): corresponding QBO composite differences (eQBO–wQBO) of $\overline{\gamma}$ (colour shaded) with climatology (grey contours). QBO zero-wind lines (solid and dashed lines) and the average location of the polar vortex edge (dotted lines) are added for location references.

Fig. 5. (a): scatter plots between the October to November averaged zonal-mean frequency of daily reversal of meridional PV gradients $\overline{\gamma}$ and the corresponding meridional PV gradient $\overline{P}_{\phi}$ at 20-45°N, 850-1250 K, where the surf zone is formed climatologically. Red stars and blue triangles indicate eQBO and wQBO winters while open grey circles indicate neutral winters. (b, c): same as (a) except for November to December and December to January averages. Note that $\overline{P}_{\phi}$ is scaled by $(\theta/350)^{-9/2}$ for consistency.

Fig. 6. (a, b): Climatology of the November to December and Feb-Mar averaged EP fluxes (arrows) and the eddy PV fluxes Π (in m s^{-1} day^{-1}) (contours). The EP fluxes have been scaled to account for their rapid decrease of magnitudes with height and to make the magnitudes of $F^{(\phi)}$ and $F^{(\theta)}$ comparable for better visualisation. All the contour lines, the thick solid and dotted lines are the same as Fig. 1. (c, d):

corresponding QBO composite differences (eQBO–wQBO). Climatological $\overline{u}$ (grey contours), QBO zero-wind lines (eQBO solid and wQBO dashed lines) and the average location of the polar vortex edge (grey dotted lines) are added for location references.

Fig. 7. (a-c): November to December averaged wave-1 EP fluxes (arrows) and the eddy PV fluxes Π (in m s^{-1} day^{-1}) (contours) for eQBO, wQBO and their differences (eQBO–wQBO) with climatological $\overline{u}$ (grey contours), QBO zero-wind lines (solid and dashed lines) and the polar vortex edge (dotted lines) added in the background. (d-f): same as (a-c) except wave-2-3. (g-i): same as (a-c) except wave-5-10. The cross-hatchings indicate statistical significance at 95% levels.

Fig. 8. Same as Fig. 7 except for Feb-Mar averages.

Fig. 9. Scatter plot between the vertical component of the EP fluxes $F^{(\theta)}$ averaged at 45-85°N, 350-450 K and the zonal-mean wind $\overline{u}$ averaged at 45-75°N, 450-1500 K. (a): both $F^{(\theta)}$ and $\overline{u}$ are Nov-Jan averages. (b): $F^{(\theta)}$ is averaged over Oct-Dec while $\overline{u}$ is averaged over Nov-Jan. Red stars and blue triangles indicate eQBO and wQBO winters while open grey circles indicate neutral winters. (c): both $F^{(\theta)}$ and $\overline{u}$ are Feb-Mar averages. (d): $F^{(\theta)}$ is averaged over Jan-Feb while $\overline{u}$ is averaged over Feb-Mar.

Fig. 10 (a): Climatology of the Nov-Jan averaged down-gradient eddy PV flux Γ (in K^2 m^4 kg^{-2} s^{-3}), where Γ is multiplied by $(\theta/350)^{-18/2}$ to be able to readily see features across the full altitude range. (b, c): QBO composite difference (eQBO–wQBO) averaged for Nov-Dec and Dec-Jan. Climatological $\overline{u}$ (grey contours), QBO zero-wind lines (solid and dashed lines) and the average location of the polar vortex edge (dotted lines) are plotted for location references.

Fig. 11. (a, b): Climatology of the November averaged zonal-mean meridional velocity $\overline{v}$ (in m s^{-1}) under eQBO and wQBO conditions, displayed in the latitudes between 30°S to 40°N. The thick solid line indicates $\overline{v}=0$. The blue arrows indicate the QBO-MMC. The purple semi-circle indicate westerly SAO that is typically enhanced under wQBO. (c): corresponding QBO composite differences (eQBO–wQBO) (coloured) with climatological $\overline{v}$ (contours). The cross-hatchings specify statistical significance at 95% levels.

Fig. 12. Schematic diagram showing the key features of RWB during eQBO (a, b) and wQBO (c, d) and in early (a, c) and late (b, d) winters. Regions of RWB are indicated red-solid upward pointing arrows with meridional dotted-wiggled arrows above. The thick-solid upward wiggling arrows that extend from the lower stratosphere into upper stratosphere indicate enhanced upward wave propagation and absorption. The thick northward pointing blue arrows indicate the PRW-driven cross-equatorial flow. See text for detailed explanations.

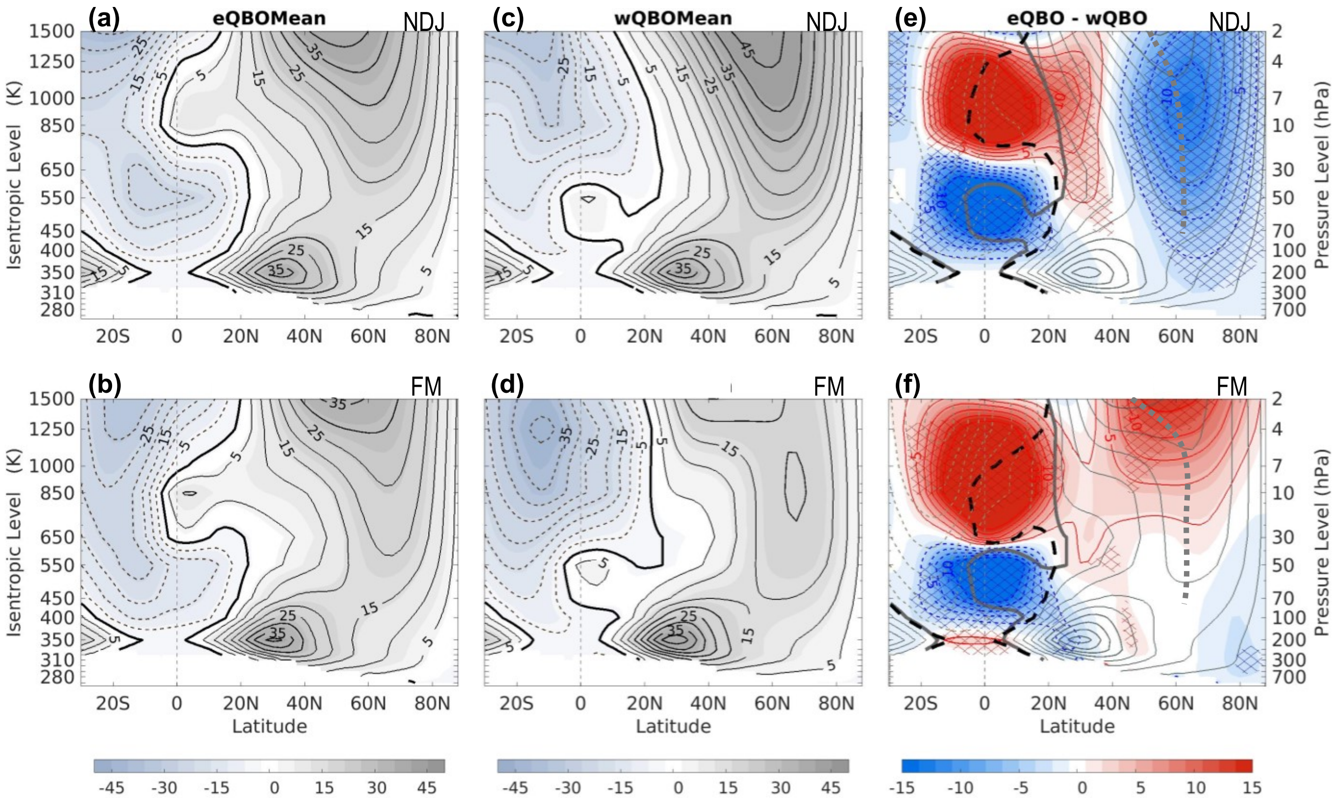

Fig. 1. (a,b): Zonal-mean zonal wind $\overline{u}$ during Nov-Jan and Feb-Mar for eQBO winter averages. Solid and dashed contours represent positive and negative winds with a contour interval of 5 m s^{1}. The zero-wind line is marked by the thick-black line. (c,d): same as (a,b) except for wQBO winters. (e,f): corresponding QBO composite differences (eQBO–wQBO) with red and blue shadings representing westerly and easterly anomalies The thick solid and dashed lines near the equator indicate the zero-wind lines for wQBO and eQBO, respectively. The average location of the polar vortex edge is indicated by the dotted lines. The cross-hatchings specify statistical significance at 95% levels.

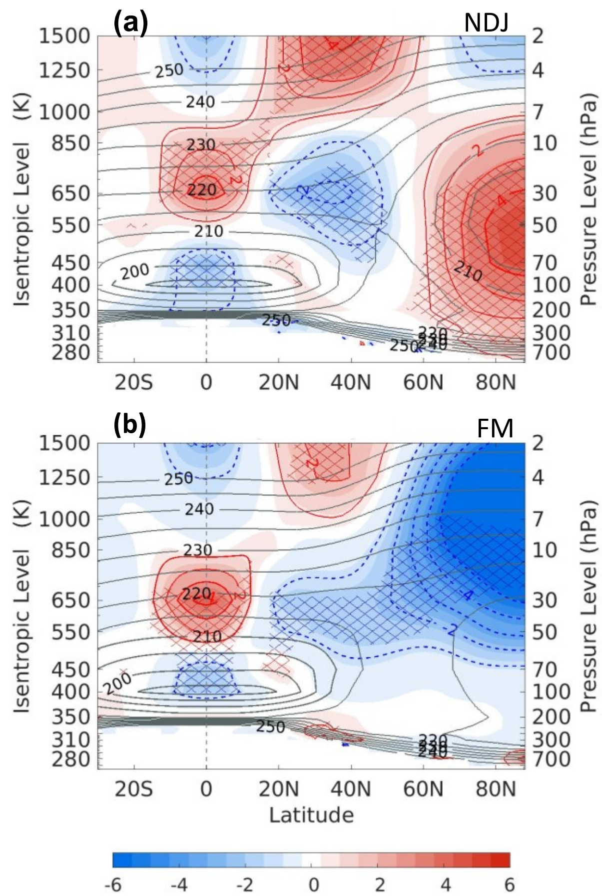

Fig. 2. Climatology (lined contours with 5°K interval) and corresponding QBO composite differences (eQBO−wQBO) of the zonal-mean temperature $\overline{T}$ during November to January (a) and February to March (b).

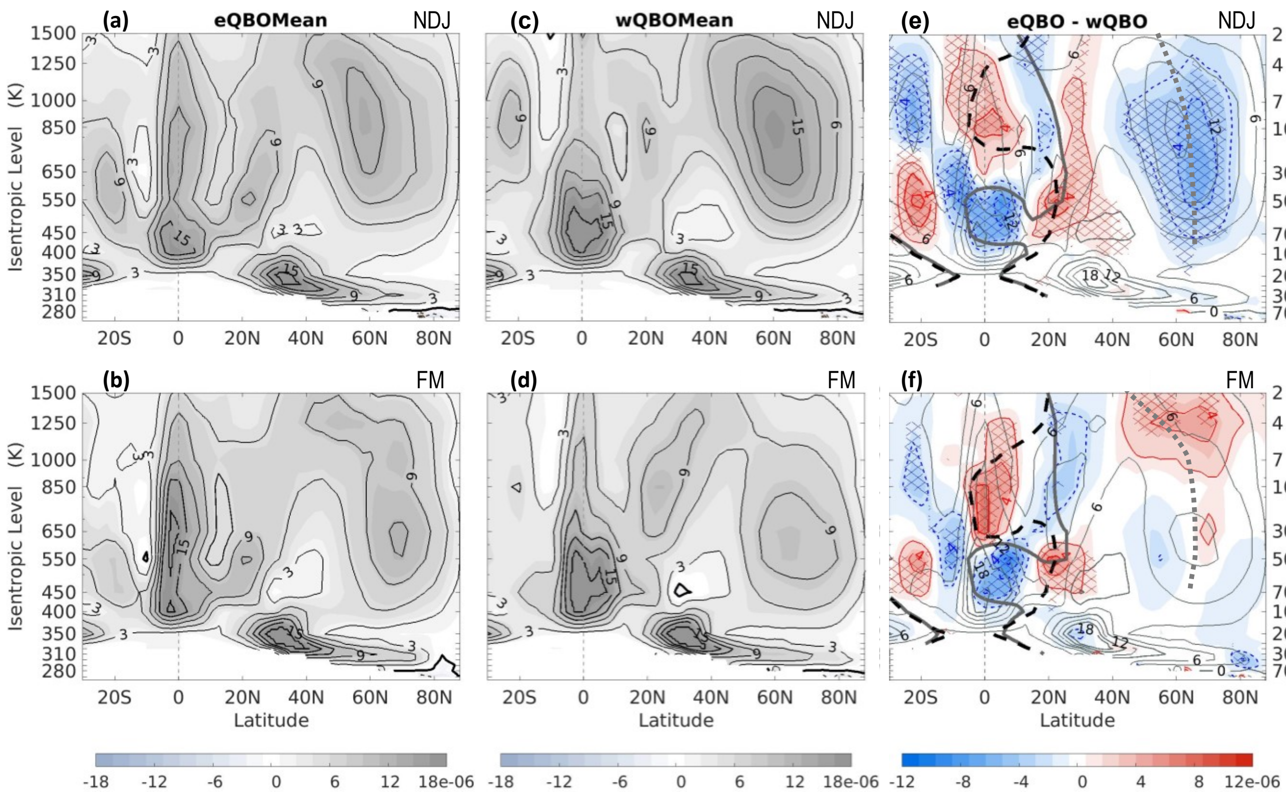

Fig. 3. (a-d): Same as Fig. 1(a-d) except for zonal-mean meridional PV gradient $\overline{P}_{\phi}$ with a contour interval of 0.25 x 10^{-5} K m kg^{-1} s^{-1}. Following Lait (1994), $\overline{P}_{\phi}$ is multiplied by $(\theta/350)^{-9/2}$ to account for its exponential increase with height. (e,f): corresponding QBO composite difference (eQBO–wQBO) of $\overline{P}_{\phi}$ (colour shaded) with climatological $\overline{P}_{\phi}$ (grey contours). The eQBO and wQBO zero-wind lines (i.e. thick solid and dashed lines near the equator) and the average location of the polar vortex edge (grey dotted line) are shown. The cross-hatchings indicate statistical significance at 95% levels.

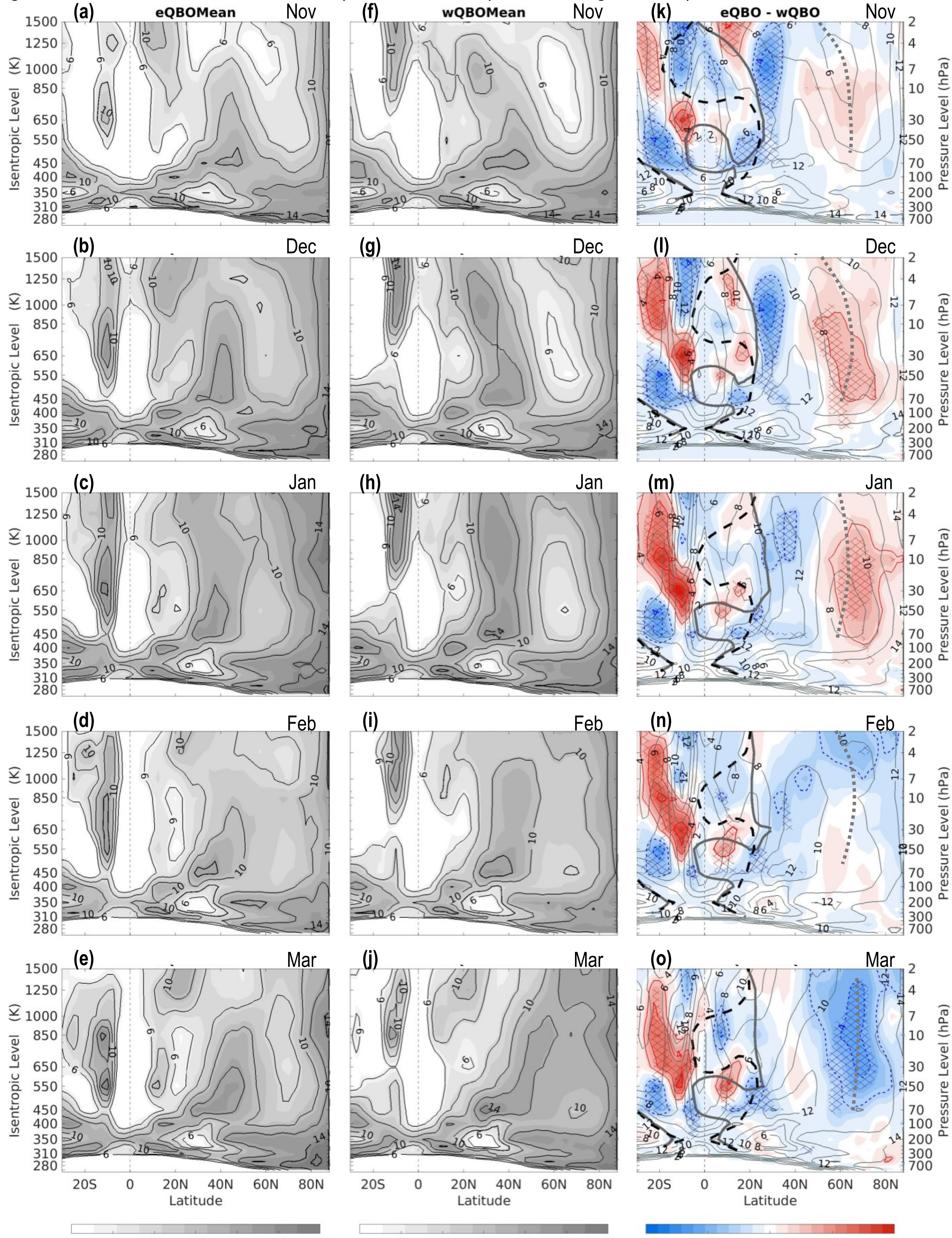
(a) eQBOMean Nov
(f) wQBOMean Nov
(k) eQBO - wQBO Nov
(b) Dec
(g) Dec
(l) Dec
(c) Jan
(h) Jan
(m) Jan
(d) Feb
(i) Feb
(n) Feb
(e) Mar
(j) Mar
(o) Mar
Isentropic Level (K)
Pressure Level (hPa)
Latitude
20S 0 20N 40N 60N 80N
1500 1250 1000 850 650 550 450 400 350 310 280
2 4 7 10 30 50 70 100 200 300 700
6 8 10 12 14 16
-8 -4 0 4 8

Fig. 4

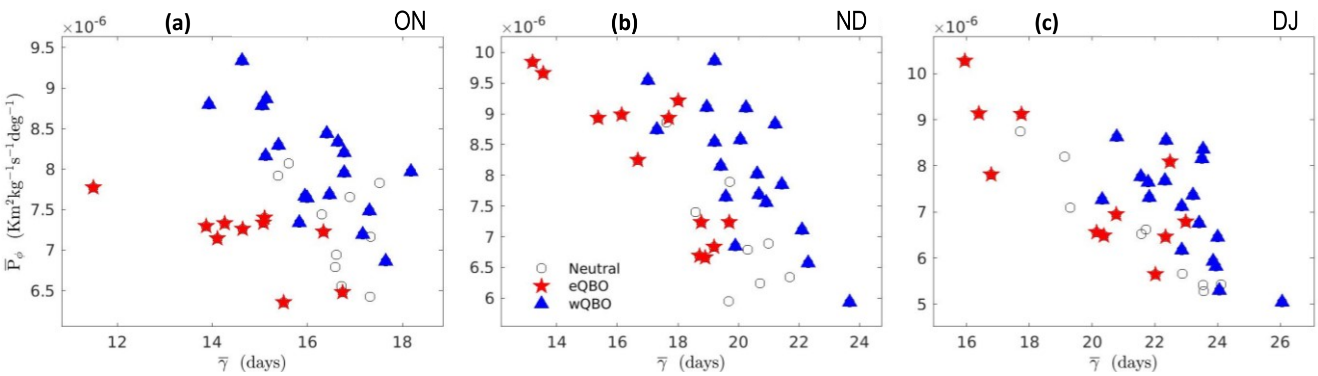

Fig. 5. (a): scatter plots between the October to November averaged zonal-mean frequency of daily reversal of meridional PV gradients $\overline{\gamma}$ and the corresponding meridional PV gradient $\overline{P}_\phi$ at 20-45°N, 850-1250 K, where the surf zone is formed climatologically. Red stars and blue triangles indicate eQBO and wQBO winters while open grey circles indicate neutral winters. (b, c): same as (a) except for November to December and December to January averages. Note that $\overline{P}_\phi$ is scaled by $(\theta/350)^{-9/2}$ for consistency.

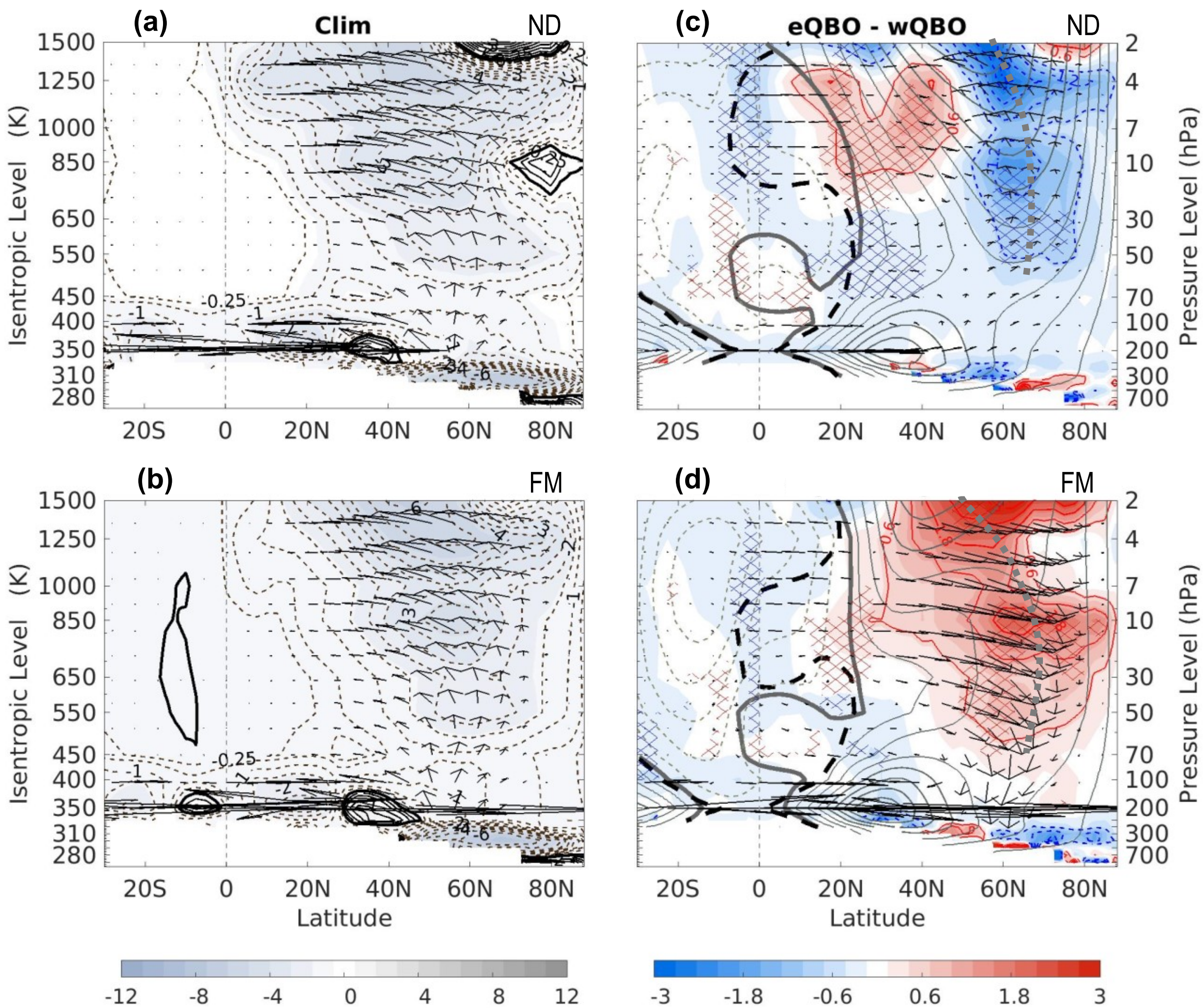

Fig. 6. (a, b): Climatology of the November to December and Feb-Mar averaged EP fluxes (arrows) and the eddy PV fluxes Π (in m s^{-1} day^{-1}) (contours). The EP fluxes have been scaled to account for their rapid decrease of magnitudes with height and to make the magnitudes of $F^{(\phi)}$ and $F^{(\theta)}$ comparable for better visualisation. All the contour lines, the thick solid and dotted lines are the same as Fig. 1. (c, d): corresponding QBO composite differences (eQBO–wQBO). Climatological $\overline{u}$ (grey contours), QBO zero-wind lines (eQBO solid and wQBO dashed lines) and the average location of the polar vortex edge (grey dotted lines) are added for location references.

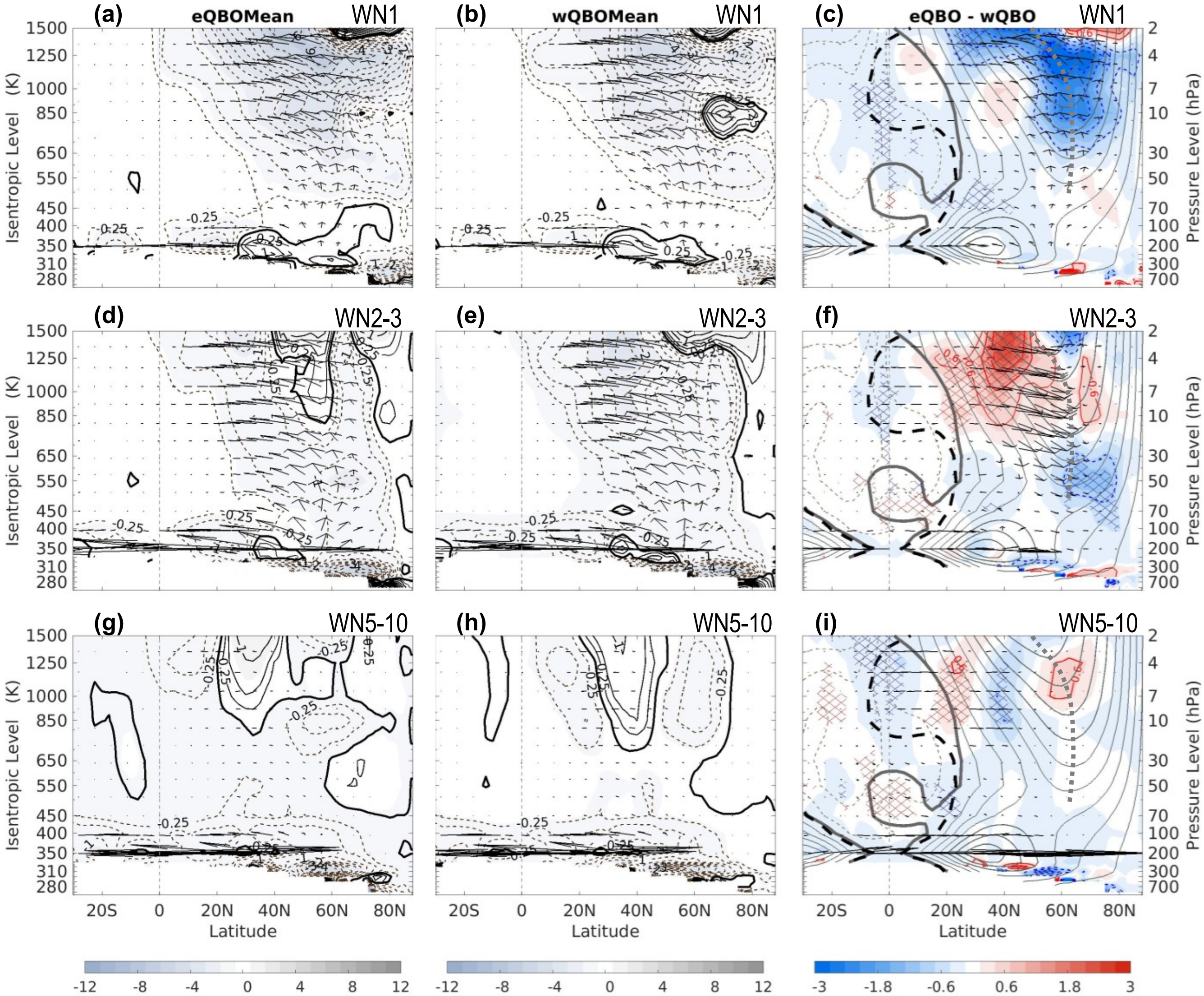

Fig. 7. (a-c): November to December averaged wave-1 EP fluxes (arrows) and the eddy PV fluxes Π (in m s^{-1} day^{-1}) (contours) for eQBO, wQBO and their differences (eQBO−wQBO) with climatological $\overline{u}$ (grey contours), QBO zero-wind lines (solid and dashed lines) and the polar vortex edge (dotted lines) added in the background. (d-f): same as (a-c) except wave-2-3. (g-i): same as (a-c) except wave-5-10. The cross-hatchings indicate statistical significance at 95% levels.

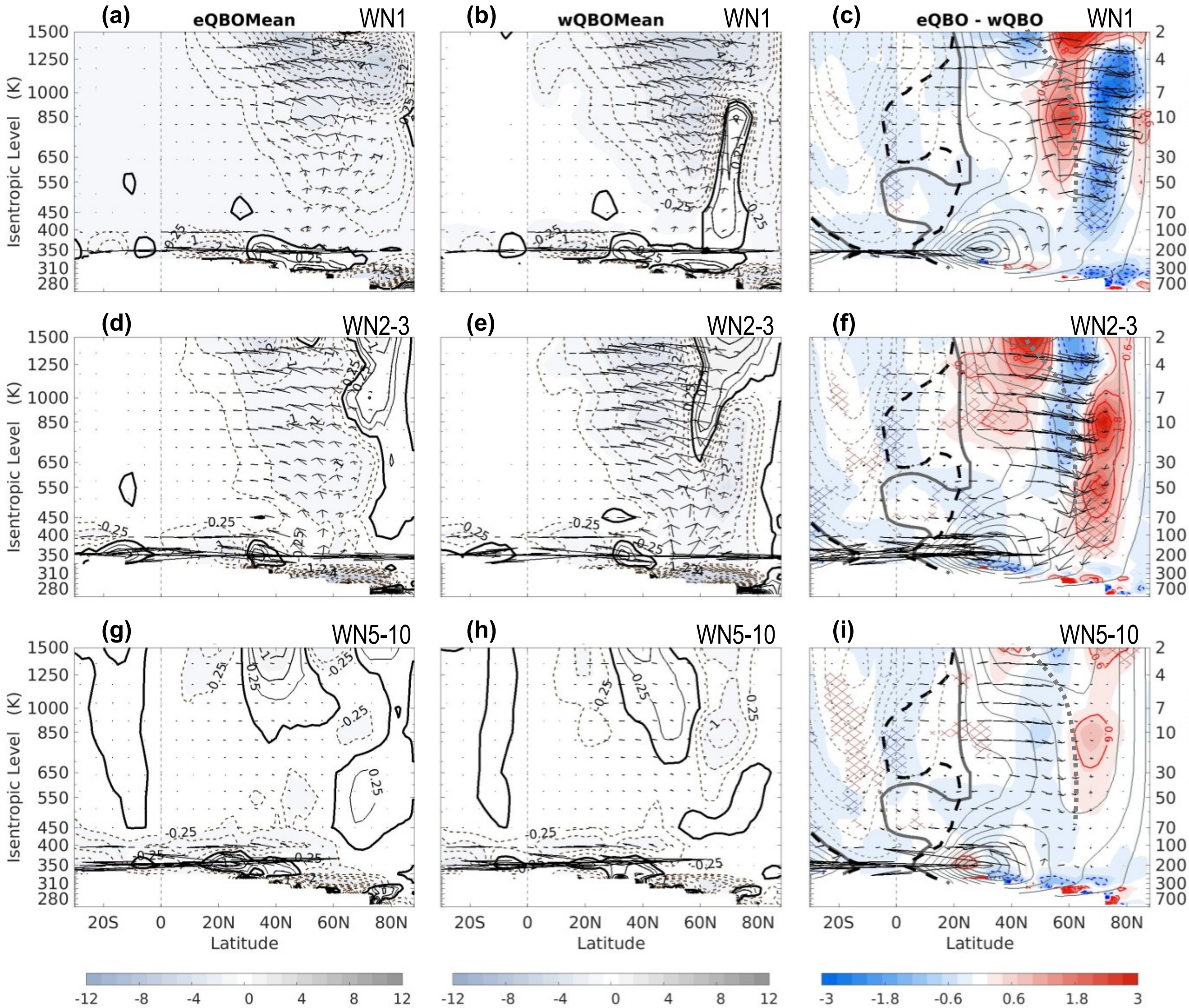

Fig. 8. Same as Fig. 7 except for Feb-Mar averages.

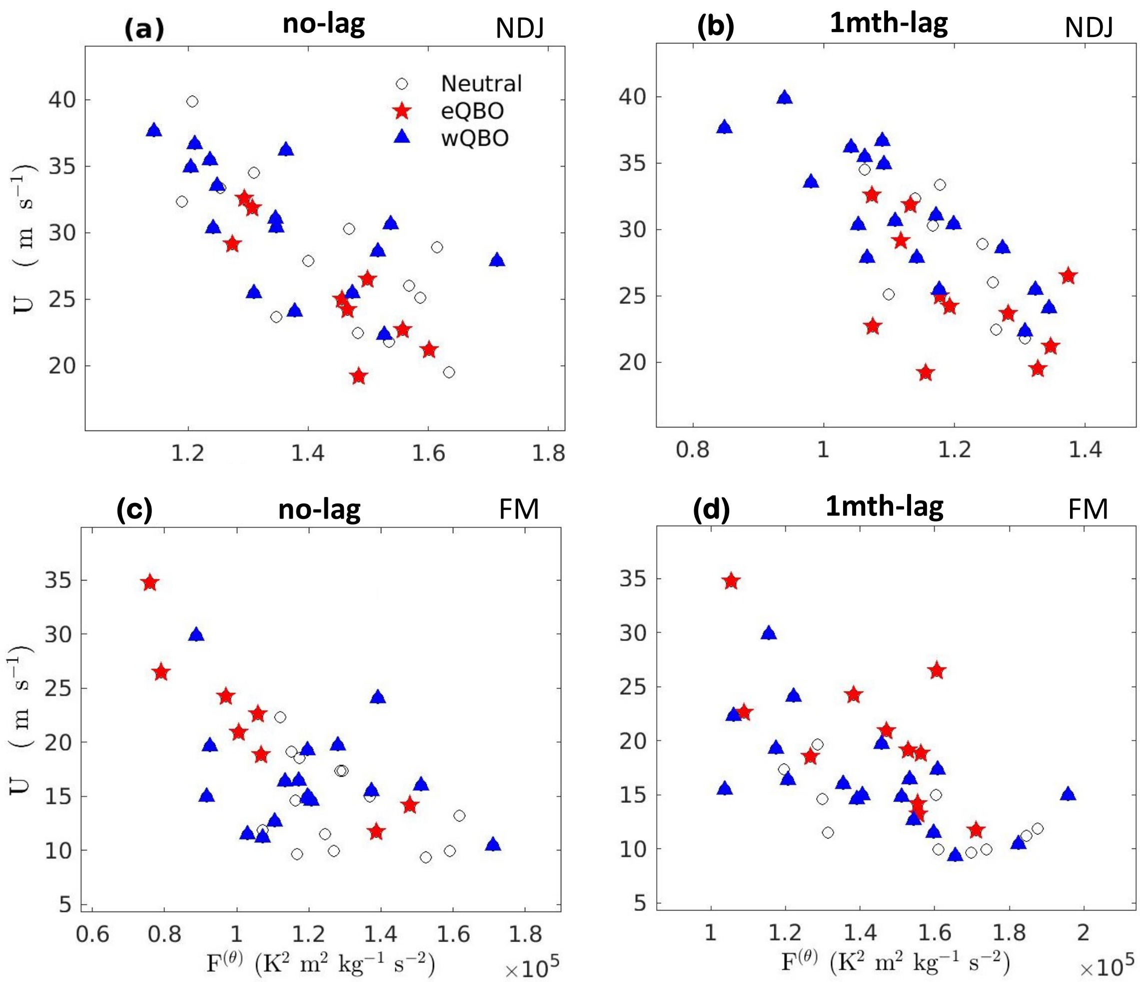

Fig. 9. Scatter plot between the vertical component of the EP fluxes $F^{(\theta)}$ averaged at 45-85°N, 350-450 K and the zonal-mean wind $\bar{u}$ averaged at 45-75°N, 450-1500 K. (a): both $F^{(\theta)}$ and $\bar{u}$ are Nov-Jan averages. (b): $F^{(\theta)}$ is averaged over Oct-Dec while $\bar{u}$ is averaged over Nov-Jan. Red stars and blue triangles indicate eQBO and wQBO winters while open grey circles indicate neutral winters. (c): both $F^{(\theta)}$ and $\bar{u}$ are Feb-Mar averages. (d): $F^{(\theta)}$ is averaged over Jan-Feb while $\bar{u}$ is averaged over Feb-Mar.

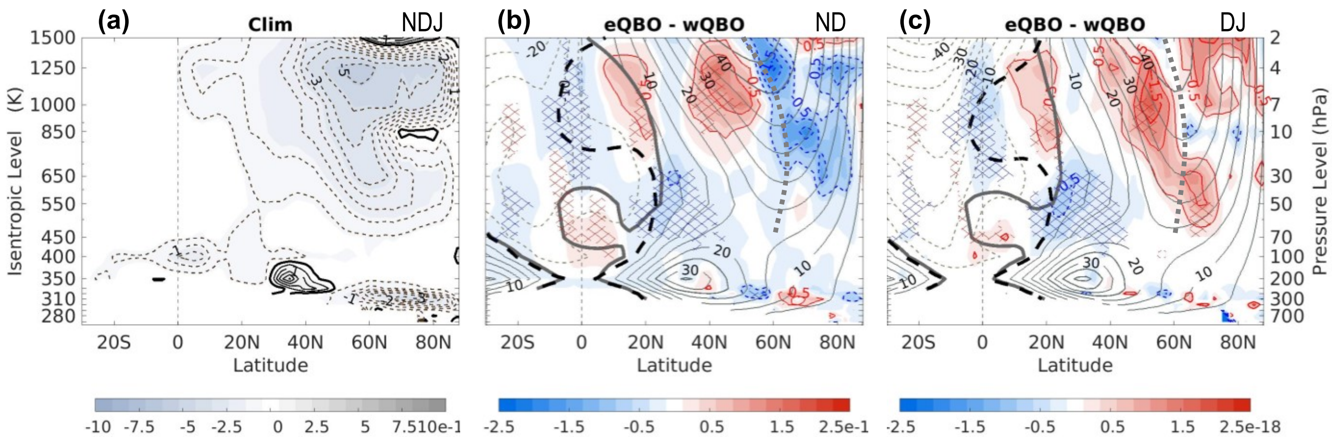

Fig. 10 (a): Climatology of the Nov-Jan averaged down-gradient eddy PV flux Γ (in $K^2\,m^4\,kg^{-2}\,s^{-3}$), where Γ is multiplied by $(\theta/350)^{-18/2}$ to be able to readily see features across the full altitude range. (b, c): QBO composite difference (eQBO–wQBO) averaged for Nov-Dec and Dec-Jan. Climatological $\overline{u}$ (grey contours), QBO zero-wind lines (solid and dashed lines) and the average location of the polar vortex edge (dotted lines) are plotted for location references.

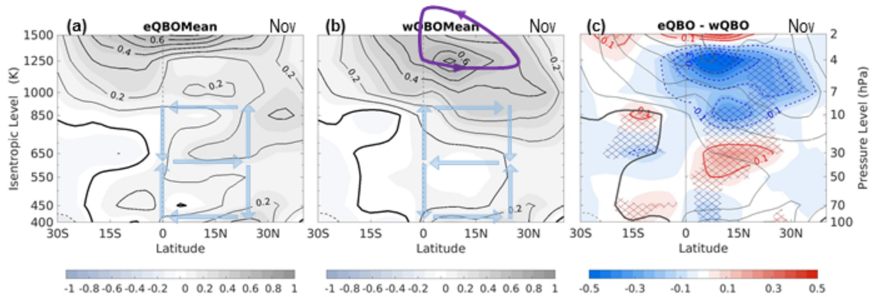

Fig. 11. (a, b): Climatology of the November averaged zonal-mean meridional velocity $\bar{v}$ (in m s^{-1}) under eQBO and wQBO conditions, displayed in the latitudes between 30°S to 40°N. The thick solid line indicates $\bar{v} = 0$. The blue arrows indicate the QBO-MMC. The purple semi-circle indicate westerly SAO that is typically enhanced under wQBO. (c): corresponding QBO composite differences (eQBO−wQBO) (coloured) with climatological $\bar{v}$ (contours). The cross-hatchings specify statistical significance at 95% levels.

190x254mm (96 x 96 DPI)

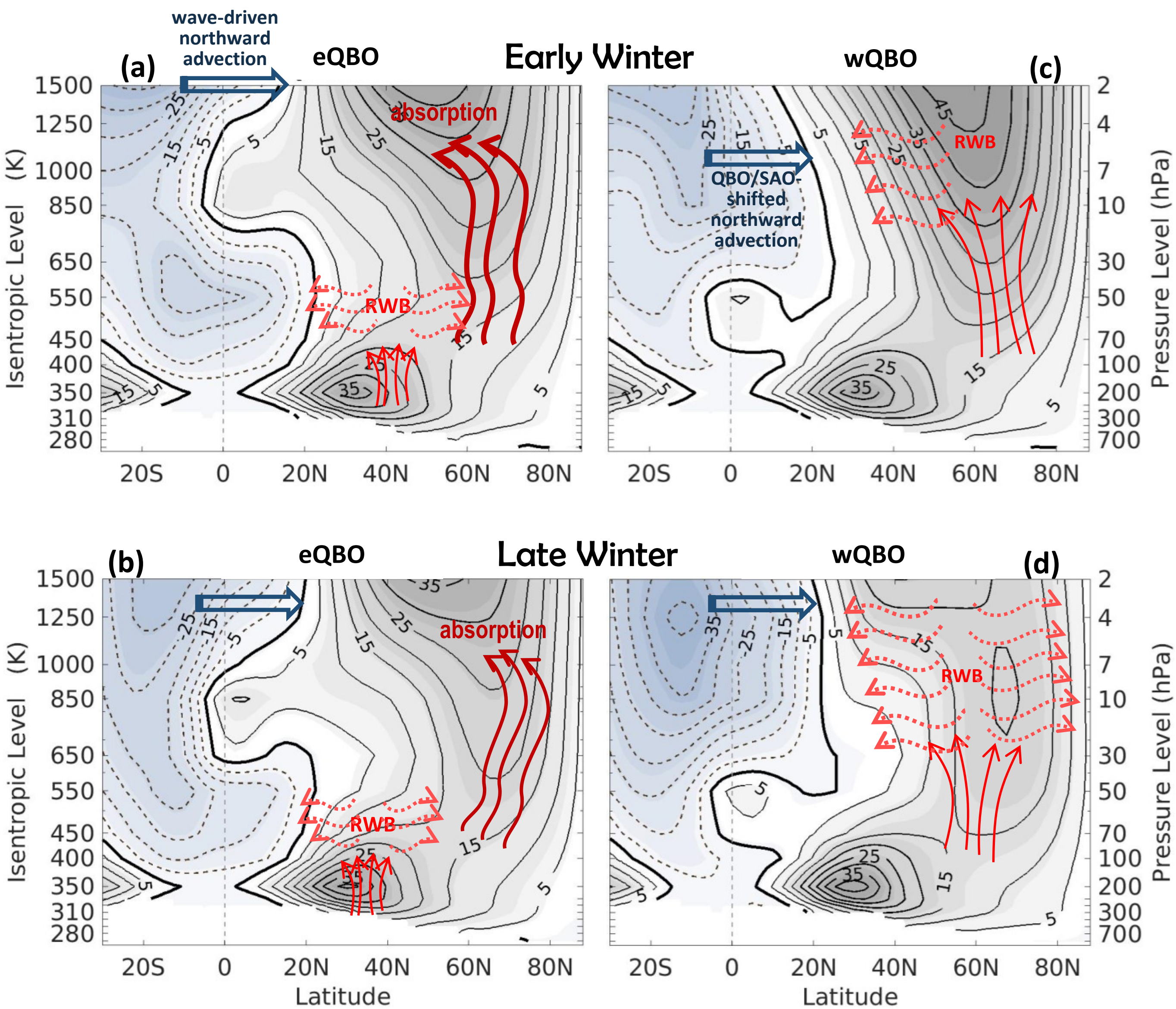

Fig. 12. Schematic diagram showing the key features of RWB during eQBO (a, b) and wQBO (c, d) and in early (a, c) and late (b, d) winters. Regions of RWB are indicated red-solid upward pointing arrows with meridional dotted-wiggled arrows above. The thick-solid upward wiggling arrows that extend from the lower stratosphere into upper stratosphere indicate enhanced upward wave propagation and absorption. The thick northward pointing blue arrows indicate the PRW-driven cross-equatorial flow. See text for detailed explanations.